Process-oriented evaluation of the West African Monsoon system in CORDEX-CORE regional climate models

Alain T. Tamoffo[1,2,4] · Alessandro Dosio[3] · Leonard K. Amekudzi[1] · Torsten Weber[4]

Abstract

Improving the simulation of the West African Monsoon (WAM) system is paramount to increasing confidence in the projections of the region's monsoon rainfall change. This work aims to thoroughly analyze the representation of the WAM system in two state-of-the-art, high-resolution (~ 25 km) regional climate models (RCMs) in order to highlight the causes of models' biases through a process-oriented evaluation approach. Model results generally feature a north (Sahel) - south (Guinea Coast) dipole-like rainfall bias, although, sometimes, positive or negative rainfall biases are evident almost over the whole of West Africa. Our analysis shows that biases in the sea- and land-surface temperature on the one hand, and biases in the sea-level and land-surface pressure, on the other hand, lead to biases in the simulated temperature and pressure contrasts between the west African landmass and the eastern Atlantic ocean. As a consequence, biases appear in the modeled monsoon flow strength, which, in turn, lead to errors in the amount of advected moisture in the interior of the continent via southwesterlies and the West African westerly jet (WAWJ) on the one hand, and the extent of deepening of the monsoon flux inland on the other hand. In addition, the African easterly jet (AEJ) is underestimated, inducing an underestimation of the African easterly waves (AEWs) activity and a weakening of the cyclonic convective circulation resulting from the AEWs' troughs, leading to a decrease in the southwesterly flow feeding mesoscale convective systems (MCSs) embedded within the AEJ. The modeled equatorward or northward shifting of the AEJ is likewise found to contribute to the models' wet or dry biases over the Sahel. Finally, there is no consistency between models and reanalyses on the one hand, and between RCM experiments on the other hand, in the way, the simulated atmospheric instability/stability modulates the convection, especially over the Sahel.

Keywords Monsoon system · Process-oriented Evaluation · Rainfall biases · West Africa · CORDEX-CORE

1 Introduction

The West African Monsoon (WAM) system is the main conveyance of the region's annual rainfall, with the maximum contribution occurring during the summer months of June–September (Diallo et al. 2014, 2016; Akinsanola et al. 2015, 2016; Sylla et al. 2015; Klutse et al. 2016; Akinsanola and Zhou 2018). Its seasonality largely influences many of the socio-economic activities over the West Africa (WA) region, such as rain-fed agriculture, hydroelectric power generation, and water resource management (Lebel et al. 2003; Odoulami and Akinsanola 2017). Although this region is identified as a climate change hotspot in Africa (Martin and Thorncroft 2013), there is no consensus amongst various ensembles of global and regional climate models on the future changes in rainfall, in terms of both magnitude and, sometimes, even sign (e.g. Cook and Vizy 2006; Dosio et al. 2020, 2021a). Therefore, assessing the plausibility of

✉ Alain T. Tamoffo
  alaintamoffotchio@gmail.com; Alain.Tamoffo@hereon.de

1 Meteorology and Climate Science Unit, Physics Department, Kwame Nkrumah University of Science and Technology, Kumasi, Ghana

2 Laboratory for Environmental Modelling and Atmospheric Physics (LEMAP), Physics Department, University of Yaoundé 1, Yaoundé, Cameroon

3 European Commission, Joint Research Centre (JRC), Ispra, Italy

4 Climate Service Center Germany (GERICS), Helmholtz-Zentrum Hereon, Fischertwiete 1, 20095 Hamburg, Germany

modeled rainfall is crucial for establishing the reliability of projections (James et al. 2018; Doblas-Reyes et al. 2021). In addition, understanding the reasons behind models' biases can be beneficial for the improvement of models' physical and dynamical formulations.

Broadly, the WAM consists of a seasonal change in the atmospheric circulation dynamics, inducing strong temporal and spatial modifications in the precipitation's pattern. This reversal in atmospheric circulation begins when the African land (Sahelian region) warms while the moist regions along the coasts of the Guinea Gulf cool down. This thermal contrast (and the consequent pressure gradient) raises moisture-laden winds from the Gulf of Guinea. Large thunderstorm systems develop when these moist winds move up onto the overheated African continent. These storms are the only annual recharge of water for the countries bordering the Gulf of Guinea and the Sahel. Moisture in the Gulf of Guinea, known as the monsoon flux, originates from southeasterlies pumped from the South Atlantic high-pressure system, and which recurve into southwesterlies while crossing the equator. The eastern Atlantic also feeds the WA via the West African Westerly Jet (WAWJ) around 10°N (Pu and Cook 2012).

The WAM is the result of a multitude of complex physical processes and mechanisms acting at diverse scales. These include remote or large-scale forcing factors such as the anomalous sea surface temperature (SST), the Pacific Decadal Oscillation (PDO), the El Niño-Southern Oscillation (ENSO) (e.g. Zhang and Zhou 2011; Diatta and Fink 2014); drivers at regional scale such as the WAWJ, African Easterly Jet (AEJ), Tropical Easterly Jet (TEJ) and African Easterly Waves (AEWs) (e.g. Cook 1999; Nicholson and Grist 2003; Akinsanola et al. 2017; Bercos-Hickey and Patricola 2021); finally, local forcings such as the surface vegetation and continental land surface conditions (e.g. Wang and Eltahir 2000; Clark et al. 2001; Sylla et al. 2016). The role of aerosols emanating from the Saharan and Sahelian regions on the WAM variability has been also established (Marcella and Eltahir 2014; N'Datchoh et al. 2018; Doblas-Reyes et al. 2021).

Numerous studies have attempted, with varying degrees of success, to model the WAM system in order to understand future changes in monsoon rainfall. Some of them are based on global climate models (GCMs) participating in the Coupled Model Intercomparison Project (CMIP-3 to 6; Meehl et al. 2007; Taylor et al. 2012; Stouffer et al. 2017), and on their multi-model ensembles (e.g. Kamga et al. 2005; Diallo et al. 2012; Monerie et al. 2012, 2021; Biasutti, 2013; Seth et al. 2013; Mariotti et al. 2014; Watterson et al. 2014; James et al. 2015). However, the GCMs' coarse grid resolution poses serious challenges to the simulation of mesoscales and local processes that modulate the monsoon system including, for instance, organized convection, land–atmosphere-ocean

interactions, surface temperature gradients, AEWs, and soil moisture (Koster et al. 2004; Cook and Vizy 2006; Watterson et al. 2014; Birch et al. 2014; James et al. 2018). Several other works (e.g. Sylla et al. 2015; Akinsanola et al. 2015; Akinsanola and Zhou 2018; Diallo et al. 2014, 2015, 2016; Klutse et al. 2016; Dosio and Panitz 2016; Dieng et al. 2017; Dosio et al. 2020) used regional climate models (RCMs) to dynamically downscale the results of CMIP5 GCMs onto a finer (~50 km) horizontal grid, within the framework of internationally coordinated activities such as the COordinated Regional climate Downscaling EXperiment (CORDEX; Giorgi et al. 2009) project, and the West African Monsoon Modeling and Evaluation (WAMMEBoone et al. 2010; Druyan et al. 2010; Xue et al. 2016) project. The downscaling is supposed to enhance the representation of smaller-scale physiographic processes while also adding local topographical information that is missing in GCMs (Giorgi and Gutowski 2015; Dosio et al 2019). In particular, the ability of RCMs to add value to the driving GCM in simulating precipitation characteristics (especially higher-order statistics) has been shown in several studies (e.g. Pinto et al. 2016; Fotso-Nguemo et al. 2017; Gibba et al. 2019) although the added value is not always clear (see e.g. Dosio and Panitz 2016). In addition, differences between model results may stem from the different configuration and parameterizations (see e.g. Sørland et al. 2021) and the "improved" precipitation field may be the result of wrongly simulated mechanisms (Tamoffo et al. 2020). Recently, a new generation of higher-horizontal resolution (~25 km) simulations has been developed within the CORDEX-Coordinated Output for Regional Evaluations (CORDEX-CORE) project (Gutowski et al. 2016). CORDEX-CORE results are designated to be utilized jointly across regions of the world for the study of regional climate processes and for the analysis of the impact of climate change on different sectors, including vulnerability assessment and adaptation options (Giorgi et al. 2021).

Some studies have already analyzed the CORDEX-CORE results over Africa. For instance, Gnitou et al. (2021) and Ilori and Balogun (2021) investigated the performances of CORDEX-CORE RCMs in simulating seasonal and annual precipitation over WA; however, these studies were merely descriptive and did not investigate the causes of RCM biases. Ashfaq et al. (2020) provided an assessment of future characteristics of monsoon systems, including the West and East African monsoon, but results were based on a single CORE RCM. Teichmann et al. (2020) analyzed the mean climate change signal at a global scale from CORE and the CMIP5 GCMs, and Coppola et al. (2021) provided an analysis of projected impact-relevant indices based on CORE, CORDEX, CMIP5 and CMIP6 runs. Finally, Dosio et al. (2021a) compared present and future precipitation daily characteristics from the available CMIP, CORDEX and CORDEX-CORE simulations over Africa. However, these studies did

not investigate the mechanisms behind differences across models' ensembles. In addition, none of these studies specifically investigated the ability of CORDEX-CORE RCMs to reproduce the WAM system, and, in particular, the mechanisms responsible for the models' biases (as done for Central Africa, by e.g. Tamoffo et al. 2021). Although the methodology is similar, given the large uncertainty in models' performances and projections over WA and where models do not agree even on the sign of future precipitation change, (see e.g. Dosio et al. 2020) a process-based analysis of RCMs focusing on WA is a very timely and critically needed.

To this end, this study aims to thoroughly analyze the representation of the WAM system in two CORDEX-CORE RCMs in order to highlight the causes of models biases by means of a process-oriented evaluation approach (James et al. 2018). The goal of the work is to highlight misrepresented physical processes associated with models' rainfall biases so as to provide guidance for their improvement. The plausibility of modeled rainfall climatology is therefore questioned in order to stimulate discussion on the fitness for purpose of RCMs, especially when their results are used to develop society's responses to the disastrous consequences of climate change. The paper is structured as follows. Section 2 describes the data and methods. The rainfall climatology of RCMs is characterized in Sect. 3. Section 4 examines how models simulate the land–atmosphere-ocean feedback. Section 5 looks at how models of the atmospheric circulation react to the land processes. The final section provides a summary and conclusions.

2 Data and methods

2.1 Modeled and observed data

In this work, two CORDEX-CORE RCMs were used: the REgional MOdel version 2015 (REMO2015; Jacob and Podzun 1997; Jacob 2001; Remedio et al. 2019) and the fourth generation of the Regional Climate Model (RegCM4-v7; Giorgi et al. 2012). Although currently, four RCMs participated in the CORDEX-CORE project, only the two models used here provided results for the entire atmospheric column necessary for the process-based evaluation. The models are run over the CORDEX-Africa domain (AFR-22) at $0.22° \times 0.22°$ horizontal resolution, using 27 vertical layers for REMO2015 and 23 for RegCM4-v7. Other details of the models' configurations are listed in Table 1. Two sets of simulations are performed: the 'evaluation' runs (1981–2010), i.e. when RCMs are driven by ERA-Interim reanalysis (Dee et al. 2011), and the 'historical' runs (1970–2005), i.e. using the results of CMIP5 GCMs as lateral boundary conditions. It should be noted that, following the CORDEX-CORE protocol, SSTs are prescribed by the driving GCMs (or reanalysis), and are not modified by RCMs, as they do not include an ocean model.

The purpose of the evaluation runs is to distinguish systematic biases (RCM internal errors) from those inherited from large-scale boundary forcing, in a "quasi-perfect forcing mode" (see e.g., Doblas-Reyes et al. 2021). The historical runs are driven by three CMIP5 GCMs, namely HadGEM2-ES, MPI-ESM-LR/MR, and NCC-NORESM1 (see more details about driving GCMs in Table 2).

Numerous observational datasets, including gauge-based, satellite-derived, and reanalysis products have been included in the analysis (Table 3). In fact, observed data feature large discrepancies over many regions in Africa. Recently, Dosio et al. (2021b) demonstrated the impossibility of using a single 'best' performing observational dataset to realistically represent rainfall features across Africa. Furthermore, they argued that assessing model results based on a very limited observational dataset may not be only pointless but can be even misleading.

For all datasets, variables utilized include precipitation, sea surface temperature (*SST*), mean sea level pressure

Table 1 Detailed configuration of CORDEX-CORE RCMs used in this study, as described in Teichmann et al. (2020)

RCMs' Names	REMO	RegCM
Model version	REMO2015 (Jacob et al. 2012; Remedio et al. 2019)	RegCM4 (Giorgi et al. 2012)
Institution	GERICS	ICTP
Resolution	0.22° X 0.22°	25 km × 25 km
Vertical levels	27	23
Map projection	Rotated pole lat-lon	Oblique Mercator
Planetary boundary layer	Monin–Obukhov similarity theory (Louis 1979)	Holtslag PBL (Holtslag et al. 1990)
Cumulus	Tiedtke (1989) with modifications from Nordeng (1994) and Pfeifer (2006)	Tiedtke (1989)
Microphysics	Lohmann and Roeckner (1996)	SUBEX (Pal et al. 2000)

Table 2 Details of the driving GCMs and names of RCM experiments used in this study

Institution	ESM	RCM (0.22° × 0.22°)	Experiment name	Period used	References
Met Office Hadley centre	HadGEM2-ES (1.25° × 1.875°)	REMO2015 RegCM4-v7	REMO-HadGEM2 RegCM4-HadGEM2	1980–2005	Collins et al. (2011)
Max Planck Institute for meteorology	MPI-ESM-LR/ MPI-ESM-MR (1.9° × 1.9°)/ (1.865° × 1.875°)	REMO2015 RegCM4-v7	REMO-MPI-LR RegCM4-MPI-MR	1980–2005	Popke et al. (2013)/ Stevens et al. 2013
Norwegian Climate Center	NCC-NorESM (1.894° × 2.5°)	REMO2015 RegCM4-v7	REMO-NorESM1 RegCM4-NorESM1	1980–2005	Bentsen et al. (2013)

Table 3 Description of the reanalysis and the satellite/gauge datasets employed for the evaluation in this study

Dataset	Institution	Horizontal Resolution	Periods used	References
CRU-TS4.04	Center for Atmospheric Research (NCAR) Climate Research Unit, University of East Anglia	0.5° × 0.5°	1980–2005	Harris et al. (2020)
GPCC-v8	Global Precipitation Climatology Centre	0.5° × 0.5°	1980–2005	Schneider et al. (2013)
Udel-v4.01	University of Delaware data	0.5° × 0.5°	1980–2005	Legates and Willmott (1990)
NIC131	New rainfall datasets recently developed for equatorial Africa	2.5° × 2.5°	1980–2005	Nicholson et al. (2019)
CHIRPS2	Climate Hazards InfraRed Precipitation with Stations	0.05° × 0.05°	1981–2005	Funk et al. (2015)
UGDP	Unified Gauge-Based Analysis of Global Daily Precipitation	0.5° × 0.5°	1980–2005	Janowiak and Xie (2011)
GPCP-v3.2	Global Precipitation Climatology Project World Climate Research Programme (WCRP)	2.5° × 2.5°	1980–2005	Huffman et al. (2009)
ARC2	African Rainfall Climatology, version 2	0.1° × 0.1°	1983–2005	Novella and Thiaw (2013)
ERA5/ERA-Interim	European Centre for Medium-Range Weather Forecasts	0.25° × 0.25°	1980–2005	Hersbach et al. (2020)/Dee et al. (2011)
MERRA2	The Modern-Era Retrospective analysis for Research and Application, version 2	0.5° × 0.66°	1980–2005	NASA (2016)
NCEP2	National Center for Environmental Prediction and the National Center for Atmospheric Research (NCAR)	2.5° × 2.5°	1980–2005	Kanamitsu et al. (2010)
HadISST2	Met Office Hadley Centre	1.0° × 1.0°	1980–2005	Titchner and Rayner (2014)
ERSST-v5	NOAA National Centers for Environmental Information	2.0° × 2.0°	1980–2005	Huang et al. (2017)

(*MSLP*), evaporation, zonal and meridional wind components (u,v), vertical wind velocity (ω), specific humidity (q), surface pressure (*SP*), air temperature (*ta*), and geopotential height (z). All variables are available at the monthly time scale from 1980 to 2005, except ARC2 and CHIRPS2 precipitation, which is available on a daily basis for 1983–2005 and 1981–2005 respectively. The meridional wind component (*v-wind*) at a daily time scale is also used to estimate the models' representation of the AEWs.

2.2 Methods

The climatology of WA (5°-20°N; 18 W°-16°E, Fig. 1) consists of a unimodal rainfall regime during the monsoon season with the precipitation peak occurring in August. Although precipitation over the coasts of the Gulf of Guinea follows a bimodal regime (Dosio et al. 2021b), here we focus on the season July–August-September (JAS), which provides the largest precipitation amount over the region, especially the Sahel, and which is the prevailing period of the WAM (Nicholson 2013).
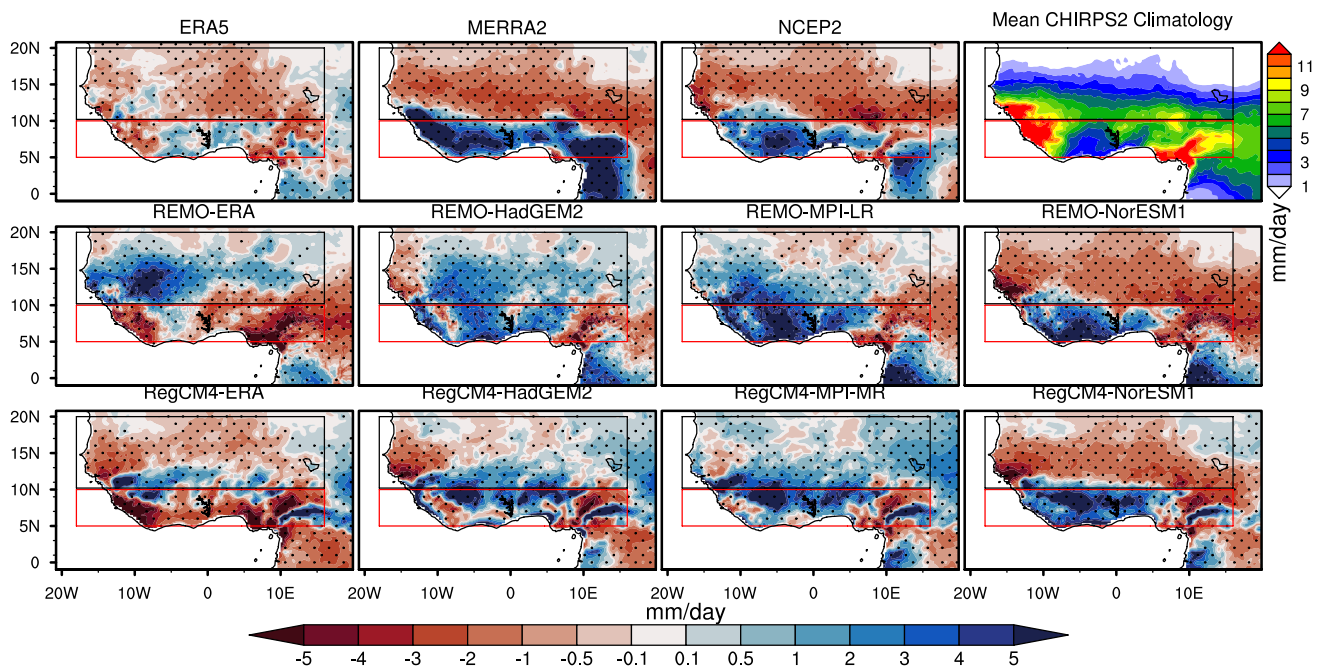
Fig. 1 Long-term mean (1983–2005) rainfall biases in the reanalysis datasets and RCM simulations (units: mm.day^{-1}). The CHIRPS2 dataset is used as reference. Stippling highlights the grid points where the rainfall bias is statistically significant at the 95% confidence level using the Student's t-test. The red and black boxes denote the Guinea Coast (18°W-16°E, 5°N-10°N) and the Sahel region (18°W-16°E, 10°N-20°N), respectively. The West Africa (WA) region (5°-20°N; 18 W°-16°E) is that resulting from the combination of the black and red boxes

First, the ability of RCMs to represent the observed spatial pattern and seasonality of rainfall is evaluated. Analyses are performed separately for the region along the coasts of the Gulf of Guinea (hereafter, Guinea Coast 18°W-16°E, 5°N-10°N; red box in Fig. 1) and the Sahel (18°W-16°E, 10°N-20°N; black box in Fig. 1). To understand the reasons behind RCMs' rainfall biases, we also evaluate the ability of the models to simulate a number of well-known drivers of the WAM system. These include land-sea interactions through *SST*, *MSLP*, *SP* variabilities and moisture transport, the dynamics of upper- and mid-tropospheric easterly jets (TEJ and AEJ), low-level westerly flows (monsoon flux), AEWs, and convection (Cook 1999; Nicholson and Grist 2003; Patricola and Cook 2007; Pu and Cook 2012; Vizy and Cook 2017; Akinsanola et al. 2017; Bercos-Hickey and Patricola 2021).

To associate rainfall biases with the atmospheric circulation, the JAS vertically integrated mass-weighted moisture transport is examined using the following equation:

$$QV = \frac{1}{g} \int_{sp}^{Ptop} qV dp \qquad (1)$$

The moisture transport *QV* can be separated into zonal (Qu in $Kg.m^{-1}.s^{-1}$) and meridional components (Qv in $Kg.m^{-1}.s^{-1}$). Similarly, the total wind speed V (in $m.s^{-1}$) is

separated into its zonal u and meridional v components. *g* is the gravitational acceleration (in $m.s^{-2}$), q is the specific humidity (in $g.Kg^{-1}$), *SP* is the surface pressure and P$_{top}$ is the pressure of the top-level (in *Pa*).

To highlight sources of moisture surplus or deficit, transient regional moisture convergence or divergence across each WA border and at each pressure level was estimated. In a given region, the total moisture convergence (divergence), i.e. the sum of inwards (outwards) moisture across the borders, can be split into the zonal (West–East; Q_λ) and the meridional (South–North; Q_φ) directions as follows (see e.g. Zheng and Eltahir, 1998):

$$Q_\lambda = \int qu d\lambda \qquad (2)$$

and

$$Q_\phi = \int qv d\phi \qquad (3)$$

where λ are longitudes and φ latitudes. The region can be considered as a rectangle of length X and width Y, X and Y being a set of segments *dl* through which the atmospheric moisture flows inwards and outwards. Thereby, moisture fluxes flowing across western ($Q_{\lambda west}$), eastern ($Q_{\lambda east}$),

southern ($Q_{\varphi south}$), and northern ($Q_{\varphi north}$) boundaries can be expressed respectively as follows:

$$Q_{\lambda west} = \int_{lwest} Q_{\lambda} dl \text{ and } Q_{\lambda east} = \int_{least} Q_{\lambda} dl \qquad (4)$$

$$Q_{\phi south} = \int_{lsouth} Q_{\phi} dl \text{ and } Q_{\phi north} = \int_{lnorth} Q_{\phi} dl \qquad (5)$$

where

dl is the distance between two grid points computed as follows:

$$dl = \theta \times \frac{\pi}{180} \times R \qquad (6)$$

with θ being the dataset's horizontal resolution in the zonal or meridional direction, and R (in m) the Earth's radius.

The integration limits are defined as.

$l_{west} = 18°W, l_{east} = 16°, l_{south} = 5°N \text{ and } l_{north} = 20°N.$

Within the integration limits, the net zonal (Q_Z), meridional (Q_M), and total (Q_T) column of the regional moisture convergence or divergence are estimated as:

$$Q_Z = Q_{\lambda west} - Q_{\lambda east} \text{ and } Q_M = Q_{\phi south} - Q_{\phi north} \qquad (7)$$

$$Q_T = Q_Z + Q_M \qquad (8)$$

As expressed in Eq. 7, positive (negative) values of Q_Z mean that inward (outward) moisture flux through the western (eastern) border 18°W (16°E) is greater than outward (inward) moisture flux through the eastern (western) border 16°E (18°W), hence the zonal moisture flux balance Q_Z is convergent (divergent). Likewise, positive (negative) values of Q_M indicate that the amount of moisture flux entering (exiting) the region via the southern (northern) boundary 5°N (20°N) is greater than that exiting (entering) across the northern (southern) frontier, hence the meridional moisture flux balance Q_M is convergent (divergent).

For identifying the AEJ and TEJ, we filtered the zonal component of the wind field and retained only the u-wind greater or equal to *6 m.s^{-1}* from the mid- to upper-troposphere following Nicholson and Grist (2003). The AEJ lies within the layers 700–600 hPa whereas the TEJ interacts around 200 hPa. For tracking the AEWs, the daily meridional wind component at 700 hPa is employed (e.g. Diedhiou et al. 1999). The signals of the atmospheric disturbances associated with the AEWs' activity are highlighted using a 2–10 day passband filter applied over the time series during the JAS season. The variance of the filtered result is then computed at each grid point to approximate the mean seasonal AEWs' activity. The large *2–10 day* temporal band is used to account for the two kinds of AEWs featuring the WA and namely *3–5* and *6–9* day period waves

(Diedhiou et al. 1998; Wu et al. 2012) as also done in previous studies by Patricola et al. (2018) and White and Aiyyer (2021).

Finally, biases in convection are examined by means of two thermodynamic metrics, namely, the moist static energy (h) and the equivalent potential temperature (θ_e) defined as:

$$h = c_p T + gz + Lq \qquad (9)$$

$$\theta_e = T_e \left(\frac{P_O}{P}\right)^{\frac{R_d}{c_p}} \approx \left(T + \frac{L_v}{c_p} r\right) \left(\frac{P_O}{P}\right)^{\frac{R_d}{c_p}} \qquad (10)$$

In Eq. 9, the first two terms on the right-hand side represent the dry static energy (DSE) input; $C_p T$ is the sensible heat, gz is the potential energy and Lq is the latent static energy (LSE); C_p is the specific heat at constant pressure, T is the air temperature, g is the gravitational constant, z is the geopotential height, L is the latent heat of condensation and q is the specific humidity. In Eq. 10, *Te* is the equivalent temperature, $P \in [1000 – 100 \ hPa]$, P_o is the standard reference pressure *(1000 hPa)*, *Rd* is the specific gas constant for air at constant pressure, *Lv* is the latent heat of evaporation and *r* is the mixing ratio of water vapor in air.

3 Characterizing RCMs' rainfall

Figure 1 shows the biases, compared to the CHIRPS2 dataset used here as reference, in long-term (1983–2005) mean precipitation for three reanalysis products as well as the RCMs simulations (both evaluation and historical runs). It is noteworthy to point out that reanalysis and RCM biases with regards to other observational products such as CRU-TS4.04, GPCC-v8, GPCP-v3.2 and the ensemble mean of all observational products, look very similar to that of CHIRPS2 (not shown). Therefore, using any of these observational products does not significantly alter conclusions. Here, CHIRPS2 is chosen as reference because of its highest horizontal grid spacing (0.05°) which allows for minimizing errors from the interpolation process. Reanalysis products are used to evaluate the RCMs' performances to reproduce the physical processes and mechanisms associated with rainfall biases. It is important to note that reanalyses are obtained by data assimilation from in-situ observational products using a reanalysis model. However, in situ stations are sparse and the density of the observation network varies from one region to another over Equatorial Africa. In regions where the surface measurement stations are widely scattered, the reanalysis data are more the result of the assimilation model than the observation station. Therefore, as for climate models, it is important to assess how well these reanalyses reproduce the observed climatology. This is also the reason why reanalysis products are used here for qualitative purposes (i.e. to assess

if the physical processes or mechanisms identified in the reanalysis data are also present in the RCM runs) rather than quantitative (i.e. to compare the intensity or magnitude of the physical processes or mechanisms between reanalyses and RCM runs) like observational products.

All reanalysis datasets and most of the RCM runs (REMO-NorESM1, RegCM4-HadGEM2 and RegCM4-NorESM1) show a north (negative) - south (positive) dipole-like rainfall bias. MERRA and NCEP show a very similar distribution of precipitation, with overestimation over the Guinea Coast and underestimation over the Sahel. The ERA5 pattern is qualitatively similar, although the magnitude of the bias is usually smaller. On the contrary, the evaluation run REMO-ERA exhibits a north (positive) - south (negative) dipole-type rainfall bias. Other simulations (REMO-HadGEM2, REMO-MPI-LR and RegCM4-MPI-MR) simulate positive rainfall biases almost over the whole of WA. Finally, the evaluation simulation RegCM4-ERA features dry biases over most parts of WA, apart from the wet biases confined within latitudes 7°–12°N.

By comparing the spatial distribution of rainfall biases of different experiments, it emerges that both the large-scale boundary conditions from GCMs and the internal physics of RCMs co-influence the results of downscaling. The influence of the boundary conditions on the RCM results is clear, as the two RCMs simulations driven by the same forcing show similar patterns of biases (although local differences exist). In particular, both RCMs simulations driven by NorESM1 show biases very similar to those of the reanalyses, whereas those driven by MPI-LR/MR show a general overestimation of precipitation. Evaluation runs show a somehow different behavior, with a general underestimation over the Guinea Coast that is not visible in MERRA-2 and NCEP2, and only visible in ERA5 over the Western coasts and the Nigeria/Cameroon's mountains. This topographic effect can indeed be missing in the lower resolution reanalyses (MERRA and NCEP). In fact, all RCM simulations show negative rainfall biases over the region. Notably, satellite products (such as CHIRPS2) have difficulties in retrieving precipitation over complex topography (Dosio et al. 2021b).

The effect of the RCM internal physical parameterization is also important. In fact, some similarities exist across the individual RCM simulations independently of the driving GCM/reanalysis. For instance, the REMO-ERA bias' pattern is different from that of RegCM4-ERA although the two experiments share a common boundary condition. Also, in all experiments (apart from those driven by NorESM1) REMO shows a larger positive bias over the Sahel compared to RegCM4, which, on the contrary, tends to underestimate precipitation, especially over the central and western regions.
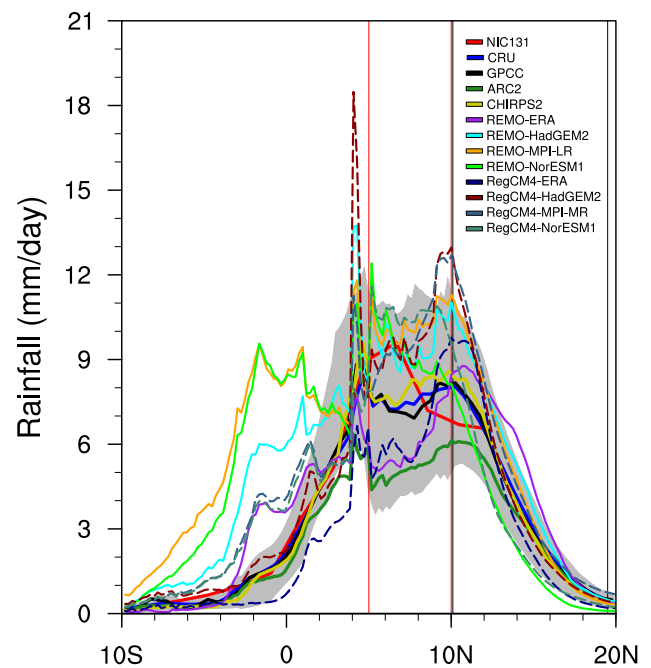

Fig. 2 Latitudinal distribution of JAS precipitation (mm.day^{-1}), spatially averaged between 18°W-16°E. Observational datasets used include rain-gauge, satellite, and combined products. The data cover the period 1980–2005, apart from the ARC2 dataset, which covers the period 1983–2005, and the CHIRPS2 dataset, which covers the period 1981–2005. Model simulations from REMO2015 (solid lines) and RegCM4-v7 (dashed lines) include both the evaluation and historical runs. The shaded gray band represents the standard deviation of the observations (CRU, GPCC, NIC131-gridded, and CHIRPS2) multi-annual means, from 1983 to 2005

JAS mean precipitation over the Guinea Coast shows large uncertainties: Fig. 2 highlights that there is little consensus across both observational products and model simulations over the region (Dosio et al. 2021b). In general, over the Guinea Coast, GCM driven RCM simulations overestimate observed precipitation (compared to CRU and GPCC, with rainfall surplus within the range 0–4.5 mm.day^{-1}. In contrast, evaluation (i.e. reanalysis driven) runs underestimate observations, especially in the region between 5° and 9°N, with rainfall deficit up to 2 mm.day^{-1}. Over the Sahel, uncertainty in both observations and model results is smaller. However, some of the model simulations (e.g. REMO-ERA, REMO-NorESM1, RegCM4-NorESM1) are, for certain latitudes, outside the range of observations. Over the ocean (latitudes < 5°N) most models tend to greatly overestimate the precipitation, especially around the Equator.

Overall, the basic pattern of the WAM rainfall climatology is well captured in the current generation of CORDEX-CORE RCMs, despite the large uncertainties in both model simulations and observational products. Observational uncertainty, associated with the low density of the

observation network in Africa (Nicholson et al. 2018), makes model evaluation of variables such as precipitation unreliable (e.g., Maidment et al. 2015; Tapiador et al. 2017, 2019; Dosio et al. 2021b). Instead, a more valuable method for model evaluation and formulation of physical parameterization is the examination of how models reproduce the

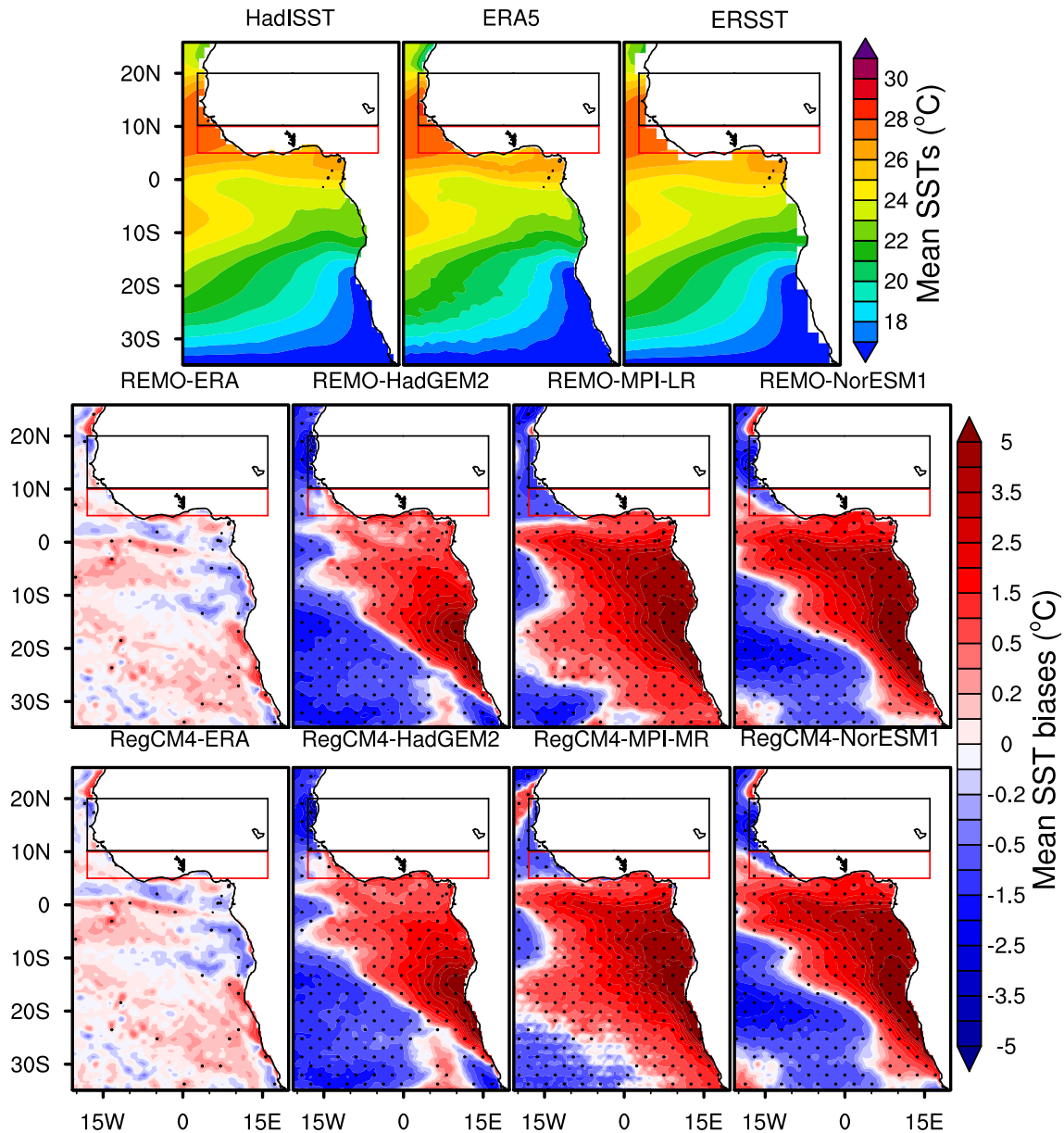physical mechanisms related to rainfall climatology (James et al. 2018). This aspect is investigated in the following sections.

Fig. 3 Mean (1980–2005) seasonal SST climatology (1st row) and models' biases (2nd and 3rd rows). The climatology is obtained from reanalysis data (HadISST, ERA5, and ERSST). The biases are computed relative to ERA5 reanalysis, from the REMO2015 and RegCM4-v7 experiments. The stippling denotes areas where the difference between the dataset under consideration and the ERA5 reanalysis dataset is statistically significant at the 95% confidence level by means of the Student's t-test

4 Land–atmosphere-ocean interactions: SST and MSLP

Figure 3 shows the mean JAS climatology of *SST* over the eastern Atlantic Ocean. All reanalyses show very consistent *SST* patterns, with the portion of the ocean bordering the most western countries featuring the highest values of *SST* (0°-10°N), in correspondence with the monsoon rainband (Fig. 1).

The evaluation simulations REMO-ERA and RegCM4-ERA feature very weakly warm **SST** biases over most of the ocean, although cold **SST** biases along the coastlines between 0° and 10°S can be noted. All the historical simulations show similar *SST* bias patterns, consisting of strong temperature overestimation over the whole Gulf of Guinea (more extended to the west of the ocean in the RCMs-MPI-LR/MR simulations), and negative *SST* biases towards the interior of the ocean. Balas et al. (2007) demonstrated the strong complexity of the relationship between *SST* and
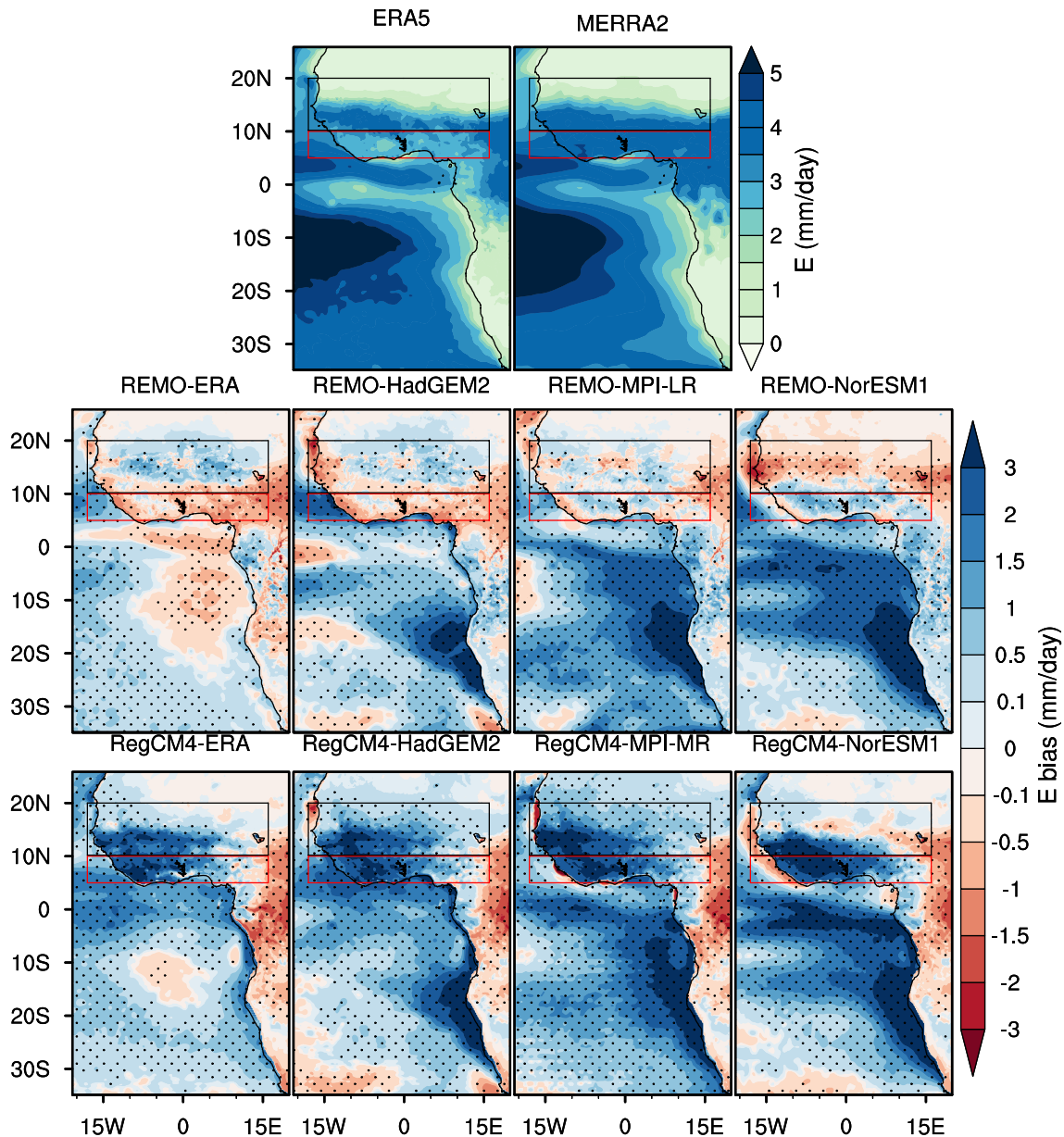

Fig. 4 Mean (1980–2005) seasonal evaporation (E in mm.day^{-1}) climatology (1st row) and E biases (2nd and 3rd rows). The climatology is obtained from the reanalysis data of ERA5 and MERRA2. The biases are computed relative to ERA5 reanalysis, from the REMO2015 and RegCM4-v7 experiments. The stippling occurs where the difference between the dataset under consideration and the ERA5 reanalysis dataset is statistically significant at the 95% confidence level by means of the Student's *t*-test

rainfall over western equatorial Africa, which is highly regionally and seasonally dependent. Factors such as general warming or cooling of the tropical oceans and Atlantic *SST* anomalies in the Gulf of Guinea are associated with precipitation anomalies over WA (Newell and Kidson 1984; Cadet and Nnoli 2007; Vizy and Cook 2001; Vizy, 2002). These authors demonstrated that positive *SST* anomalies enhance the evaporation over the Gulf of Guinea, which in turn, strengthens northward moisture advection into WA, despite the weakening of the meridional temperature gradient. While this process increases precipitation over the Guinea Coast, it rather reduces precipitation over the Sahel because the subsidence strengthens over the equator in order to compensate for the potential vorticity. Therefore, we next verified whether warm SST biases prescribed by driving GCMs are accompanied by increased evaporation.

Figure 4 displays the mean climatology of evaporation from ERA5 and MERRA2, together with the RCMs' evaporation biases relative to ERA5. Apart from the evaluation run REMO-ERA, which shows negative biases over nearly the whole Gulf of Guinea, all the other simulations feature strong positive biases over the most part of the eastern Atlantic Ocean. Over land, experiments from REMO2015 show evaporation bias patterns very different from those of RegCM4. REMO-ERA and REMO-HadGEM2 simulate a north (Sahel, positive) - south (Guinea Coast, negative) dipole-like evaporation bias that is reversed in REMO-NorESM1. REMO-MPI-LR features a prevalence of slight positive biases in most parts of WA. On the other hand, most of the RegCM4 experiments show strong positive biases in the entire WA except RegCM4-ERA and RegCM4-NorESM1, which show negative biases in a small portion of the northern Sahel. Differences in the patterns of evaporation biases of the two RCMs over the Sahel might induce differences in atmospheric circulation. In fact, the underestimating of evaporation in REMO experiments may indicate amplified warming over the Sahel, owing to the limited latent heating necessary to cool land surface and to distribute heat to the atmosphere, thereby contributing to modify meridional temperature gradients despite warm biases of SST over the Guinea Gulf (Vizy and Cook 2017). On the contrary, the overestimating of evaporation in RegCM4 runs might induce opposite effects. These assumptions will be verified in Sect. 5. Notably, rainfall bias patterns are somehow similar to those of the evaporation in overall RCM experiments (see Fig. 1): in fact, the increase in rainfall causes an increase in soil moisture, which, in turn, increases evaporation because of unsaturated soils.

Another important process modulating the land-atmosphere-ocean feedback is the variability in MSLP and SP. In fact, the land-sea thermal contrast (∇T) induces a land-sea pressure gradient (∇P) that enhances low-level westerly

and southwesterly moisture transport inland, and, eventually, precipitation (Patricola and Cook, 2007; Vizy et al. 2013). Figure 5 highlights that, except RegCM4-ERA which slightly overestimates MSLP, all other simulations underestimate it, including the South Atlantic High-pressure system (20°–30°S), in part or in full. Figure 6 reveals that although all simulations adequately reproduce the seasonality of the land-ocean temperature and pressure contrasts (∇T, ∇P), most RCMs simulate a weaker ∇T relative to ERA5 and MERRA2. Consequently, most models underestimate ∇P, especially at the monsoon onset (June–July) compared to ERA5, and during all the monsoon time (JJAS) compared to MERRA2. A direct consequence of differences in ∇T and ∇P between model runs is the difference in the amount of moisture imported into land regions, associated with the strength of the monsoon flow. In fact, weak temperature and pressure gradients weaken the monsoon flow, reducing the amount of inwards moisture, thereby suppressing convection, especially over the Sahel where moisture availability is limited. Conversely, strong land-ocean thermal and pressure gradients displace advected moisture from the ocean further into the continent, therefore weakening (strengthening) the moisture availability over the Guinea Coast (Sahel), and hence convection. Modeled biases in ∇T and ∇P might also affect the simulated West African westerly jet (WAWJ; Pu and Cook 2012), which is responsible for moving moisture from the eastern Atlantic onto the WA. This is discussed in the following section.

5 The response of the atmospheric circulation

We first examine how RCMs simulate the regional atmospheric column moisture availability (Fig. 7). The total column moisture convergence/divergence (*QT*) is separated into the zonal (*QZ*) and meridional (*QM*) components to comprehensively identify sources of biases. Reanalyses and RCM runs agree on the shape of the vertical profile of moisture content in all components, but differences in intensity remain. Uncertainties are larger for *QZ* than *QM* in mid-layers. In the bottom layers, reanalysis products and RCMs show large variations in all components of the convergence/divergence. For instance, all models overestimate moisture convergence for *QZ* between 950 and 700 hPa compared to ERA5 (and partly NCEP2). In particular, some RCMs do not show any divergence in the entire column. REMO-ERA shows a profile of *QZ* very close to that of ERA5 between 925 and 700 hPa, whereas RegCM-ERA shows very small values of convergence/divergence for the entire column, similar to MERRA2. In the *QM* component, REMO runs and the NCEP2 reanalysis are closer along the tropospheric column compared to other
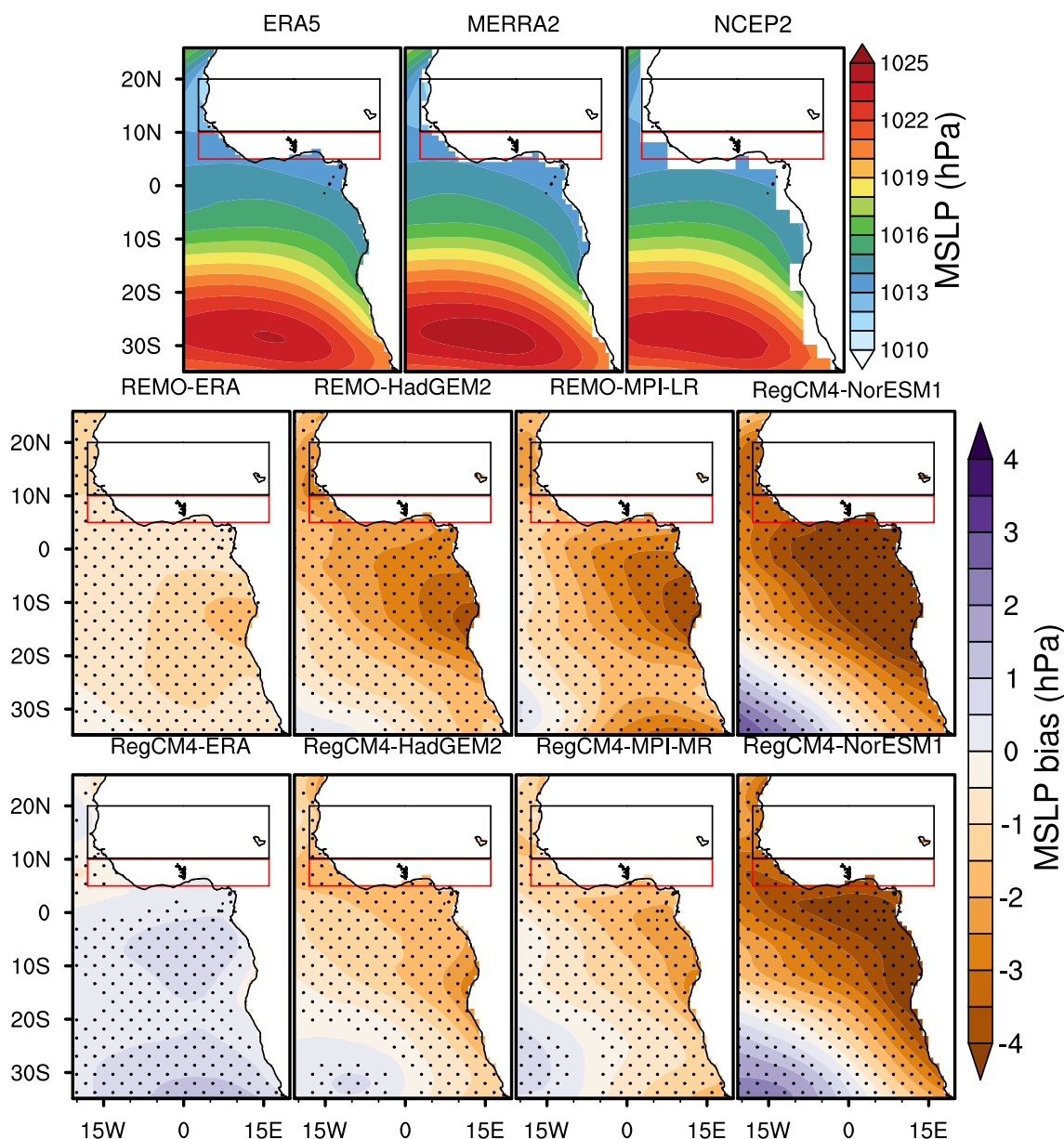
Fig. 5 Mean (1980–2005) seasonal SLP climatology (in the top row) and SLP biases (in the middle and bottom rows). The climatology is obtained from reanalysis data (ERA5, MERRA-2, and NCEP2). The biases are computed relative to ERA5 reanalysis, from REMO2015 and RegCM4-v7 experiments. The stippling occurs where the difference between the dataset under consideration and the ERA5 reanalysis dataset is statistically significant at the 95% confidence level by means of the Student's *t*-test

reanalysis datasets. They feature moisture convergence from the bottom layers up to 700 hPa and slight moisture divergence between 700 and 600 hPa. RegCM4 simulations show stronger moisture convergence at 850 hPa relative to all reanalyses and REMO simulations, and become similar to REMO and reanalyses in other layers, apart from RegCM4-ERA which models moisture divergence around 850 hPa. Therefore, strong moisture convergence in QT in lower layers (1000–850 hPa) is a result of both QM (strong) and QZ (weak). QT is divergent in mid-layers

(800–500 hPa), as a result of divergence in QZ (strong) and QM (weak).

To understand the reasons behind these differences, the ability of models to properly distribute moisture across WA is assessed in Fig. 8. Results show that stronger low-level QZ is associated with stronger modeled WAWJ and low-level westerlies over the coast of the Gulf of Guinea. Also, a stronger low-level QM is related to a large amount of southeasterlies turning into southwesterlies while crossing the Guinea Gulf. However, patterns of the zonal integrated

Fig. 6 Seasonality of the near-surface **a** land–ocean temperature difference (thermal contrast; ∇T; K) and **b** land-surface pressure and ocean sea-level pressure difference (∇P; hPa) between the interior of the continent (15°W-16°E, 10°-30°N) and the southeastern Atlantic Ocean (15°W-16°E, 0°–20°S), for the ERA5 (red), MERRA-2 (black), and NCEP2 (blue) reanalysis data, and for the REMO2015 (solid lines) and RegCM4-v7 (dashed lines) experiments, over the period 1980–2005
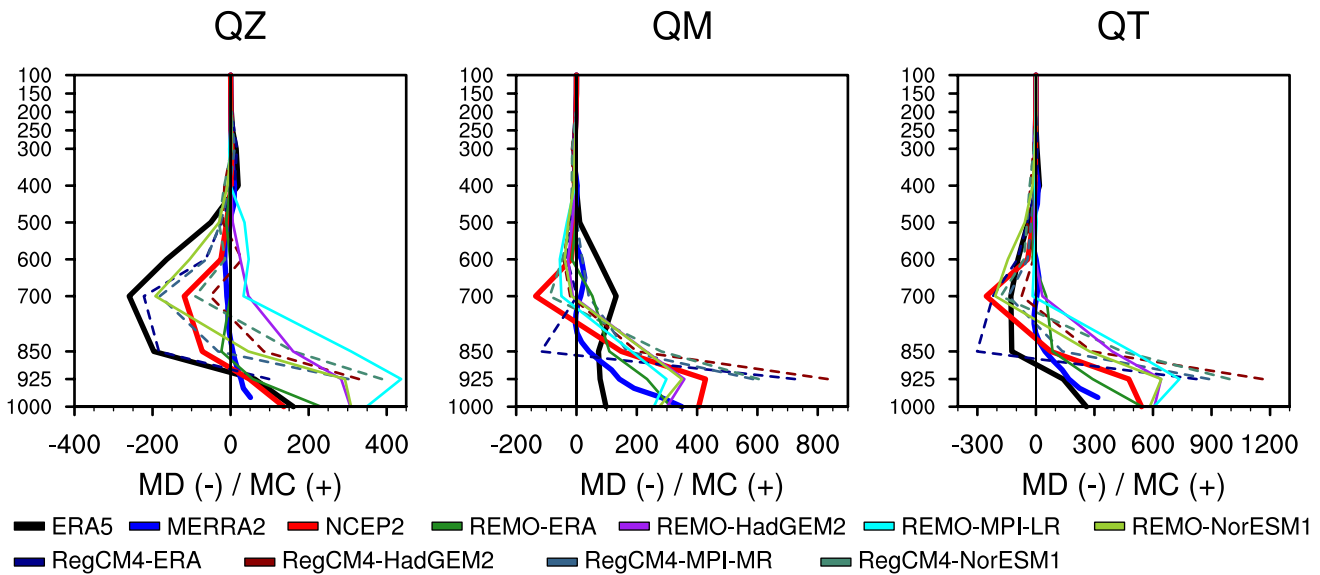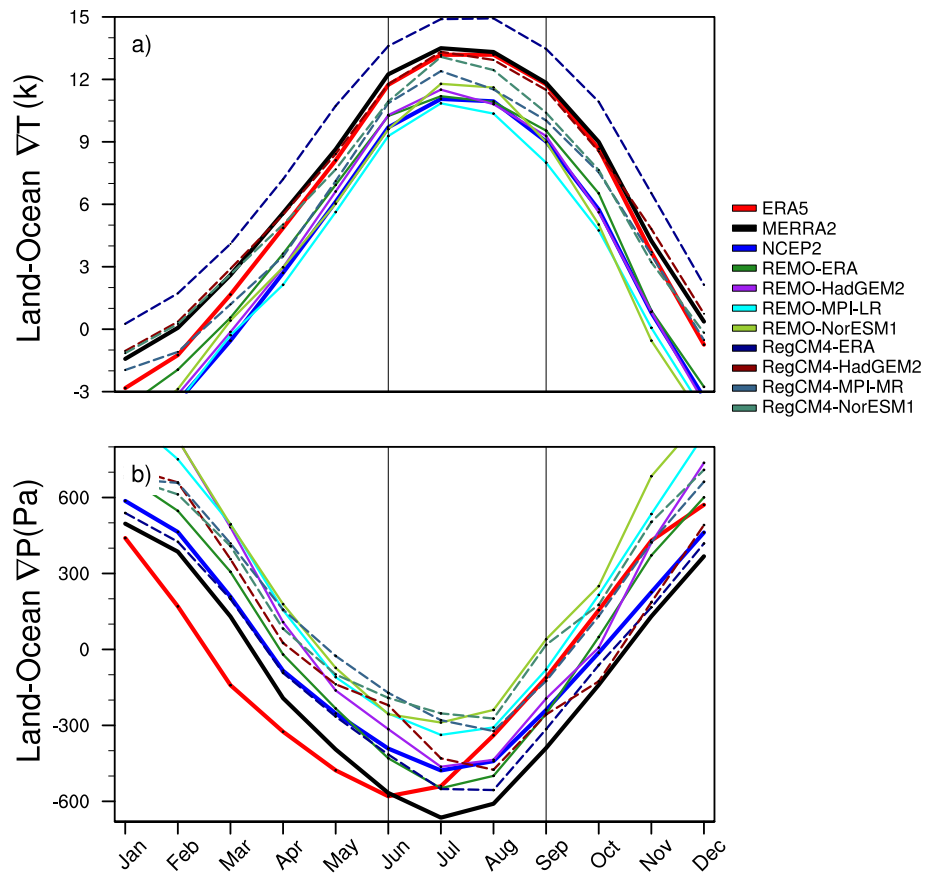

Fig. 7 Vertical profile of the regional moisture convergence/divergence (kg.m^{-1} s^{-1}) across the WA, divided into the (left) zonal (QZ) and (centre) meridional (QM) directions. (right) The total column moisture convergence/divergence (QT); MD = moisture divergence (negative values) and MC = moisture convergence (positive values). Data used are from reanalyses ERA5 (black), MERRA-2 (blue), and NCEP2 (red), and from experiments REMO2015 (solid lines) and RegCM4-v7 (dashed lines) over the period 1980–2005
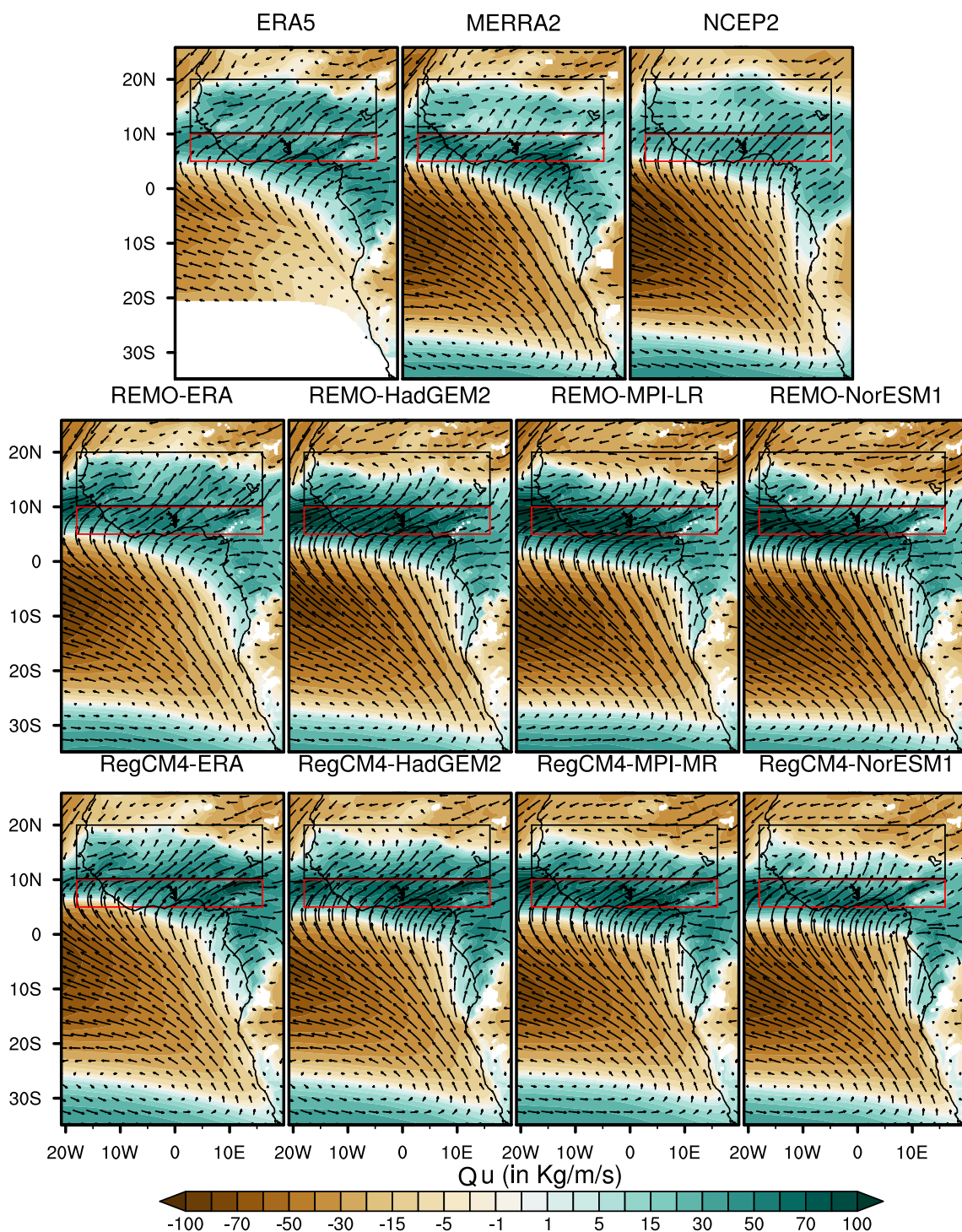
Fig. 8 Mean (1980–2005) seasonal climatology of lower-layer (1000–850 hPa) zonal vertically integrated moisture flux (Qu; kg.m^{-1} s^{-1}; shaded) superimposed with vertically integrated (1000–850 hPa) total moisture transport (QT; kg.m^{-1} s^{-1}; vectors). Data used are from rea-nalyses (ERA5, MERRA-2, and NCEP2) and from the REMO2015 and RegCM4-v7 experiments. Negative values indicate easterly flows and positive values are westerly flows

moisture transport (*Qu*) reveal divergences between simu-lations. In fact, REMO-ERA is close to reanalysis data with a widespread area of positive *Qu* covering the entire Guinea Coast and the Sahel. The RegCM4-ERA *Qu* pat-tern is instead similar to those of the historical simula-tions, consisting of higher positive but less widespread

Qu values in the Sahelian region. It is worth noting that some simulations (e.g. REMO-HadGEM2, RegCM4-MPI-MR) that feature precipitation wet biases over the Sahel (Fig. 1), show total moisture transport and *Qu* similar to those featuring dry biases (e.g. RegCM4-ERA). Also, reanalysis products that feature strong precipitation dry biases in the Sahel, feature further inward moisture into the region, which is not the case for some experiments (e.g. REMO-NorESM1, RegCM4-NorESM1) featuring dry biases over the Sahel, but accompanied with little moisture convergence onto the region. This suggests that the low-level circulation is not the only process causing differential wetting/drying between datasets.

We, therefore, investigated other processes driving the WAM system. The African Easterly Jet (AEJ) and the Tropical Easterly Jet (TEJ) are of great importance in modulating moisture transport in mid- (700–600 hPa) and upper (around 200 hPa) tropospheric layers respectively. The AEJ modulates the development of the rainy season by increasing/decreasing the number of mesoscale convective systems (MCSs). This is also associated with a strong/weak baroclinic instability over the Sahel (Nicholson and Webster 2007). In turn, rainfall feedback on the jet through strengthening or weakening in the meridional surface temperature gradient; the strong TEJ can accentuate the convective

activity by increasing upper-level divergence, thereby favoring ascent motions in the bottom layers that leads to high rainfall over the Sahel (Grist and Nicholson 2001; Nicholson and Grist 2003; Nicholson and Klotter 2020; Bercos-Hickey and Patricola 2021). The vertical profile of zonal wind is thereby shown in Fig. 9, where the AEJ and TEJ are also highlighted. REMO simulations are generally closer to reanalyses compared to RegCM4 ones. In fact, according to all reanalysis datasets, the mid-tropospheric AEJ shows a strong (> 14 m.s⁻¹) core located over the Sahel, around 15°N. At the same time, the upper-tropospheric TEJ core (> 16 m.s⁻¹) is located over the Guinea Coast (around 5°N). REMO runs simulate weaker AEJ and TEJ compared to all reanalyses, with differences ranging within 2–4 and 4–6 m.s⁻¹ respectively. All RegCM4 runs show only a very weak AEJ, and a southward shifting and underestimated TEJ core. Two distinct processes are associated with models' wetness and dryness over the Sahel and seem to be driven in major part by the AEJ: the poleward or equatorward shifting of AEJ and the jet strength. In fact, experiments that feature rainfall dry biases simulate an anomalous equatorward AEJ (e.g. REMO-NorESM1, RegCM4-ERA, RegCM4-NorESM1); those simulating precipitation wet biases experience a weaker and northward AEJ (e.g. REMO-ERA; REMO-HadGEM2; RegCM4-MPI-MR). This is consistent
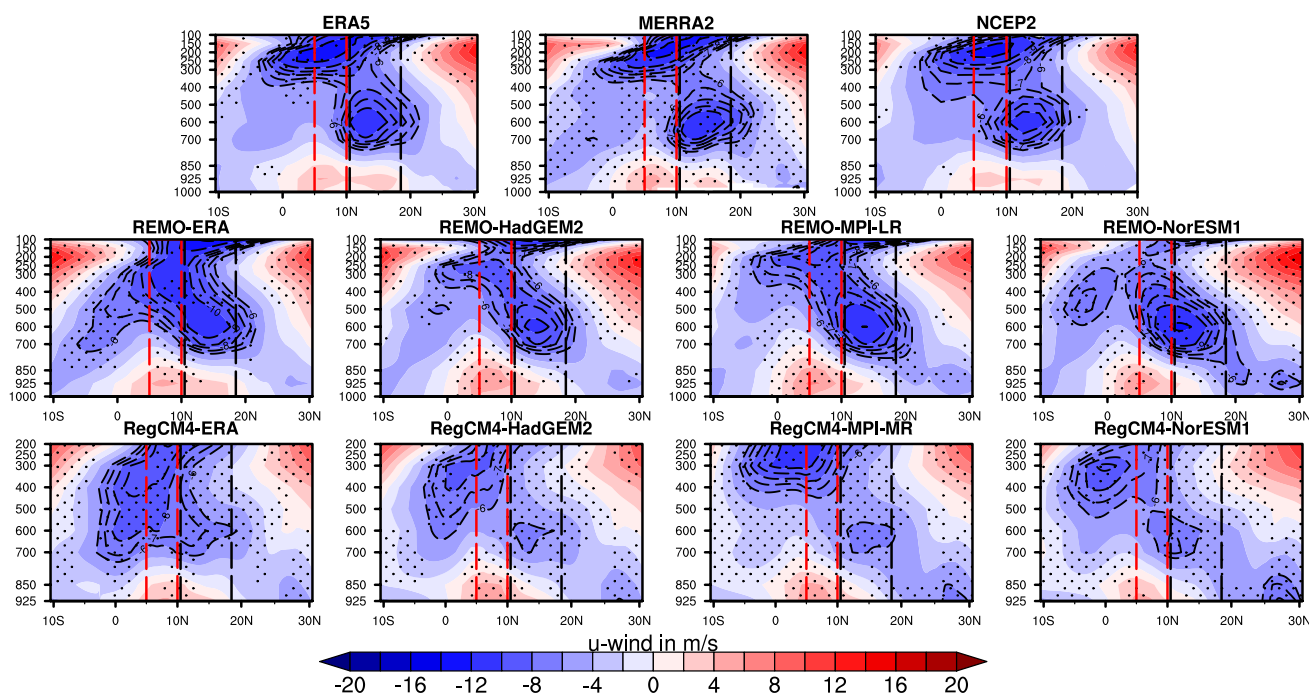

Fig. 9 Latitude-height cross-sections of zonal wind (*u-wind*; m.s⁻¹; shaded), averaged over longitudes 10°W-10°E (following Nicholson and Grist, 2003). Overlaid dashed contours indicate the mean seasonal location of AEJs (wind speed > 6 m.s⁻¹). Data used are from the reanalyses ERA5, MERRA-2, and NCEP2 and the experiments REMO2015 and RegCM4-v7, from 1980 to 2005. The stippling occurs where the difference between the dataset under consideration and the ensemble mean of the three reanalysis products is statistically significant at the 95% confidence level by means of the Student's *t*-test. The red bars define the Guinea Coast and the black bars denote the Sahel

with previous findings by Nicholson and Webster (2007) who showed that an equatorward (poleward) shifting of AEJ may promote moisture divergence (convergence) from (into) the region, therefore suppressing (enhancing) convective activity due to the reduced (increased) moisture availability. The rainfall dry biases over the coasts of the Gulf of Guinea in the two evaluation experiments (REMO-ERA and RegCM4-ERA) are related to stronger (compared to all reanalyses) mid-level tropospheric easterly divergence. This process dries mid-layers and probably reduces MCSs thereby weakening the convection.

Figure 9 also shows that in the lower layers (> 850 hPa), the extent to which the models simulate the penetration of the monsoon flow inland differentiates the experiments that represent wet biases over the Sahel from those that represent dry biases. In the first case, the monsoon flux deeply enters the continent up to 13°N (REMO-ERA, REMO-HadGEM2, REMO-MPI-LR). Although the absence of the model outputs at 1000 hPa pressure level makes it difficult to analyze the RegCM4 runs, this would be the case for RegCM4-MPI-MR. In the second case, the strength of the monsoon flow is weak, resulting in a less inland penetration of moisture and therefore an unevenly distributed moisture across the region

(RegCM4-ERA, RegCM4-HadGEM2, REMO-NorESM1 and RegCM4-NorESM1).

The coupling between the AEJ and AEWs is well known, as well as the role AEWs play in the Sahel rainfall system (Fink and Reiner 2003; Nicholson 2013). Indeed, the existence of AEWs was first attributed to a joint baroclinic-barotropic instability associated with the vertical and horizontal shear of the AEJ during the monsoon time from June to October (Nicholson and Grist 2003). Newer studies showed that AEWs may require a genesis mechanism such as convection coupled with the AEJ's instability (Thorncroft et al. 2008; Leroux and Hall 2009). AEWs are the main precursor of the Atlantic tropical cyclone genesis and strongly modulate mesoscale deep convection (Dieng et al. 2014). We discussed previously the biases in the modeled AEJ, which may indicate biases in simulated AEWs. The way the models represent the mean seasonal climatology of the AEWs' activity is illustrated in Fig. 10 through the variance of the 2–10 day passband filtered meridional component of the wind (note that the daily meridional wind component is not available for REMO2015 RCM, therefore, only results based on RegCM4-v7 experiments are shown). Biases in the modeled AEWs' activity are consistent with simulated
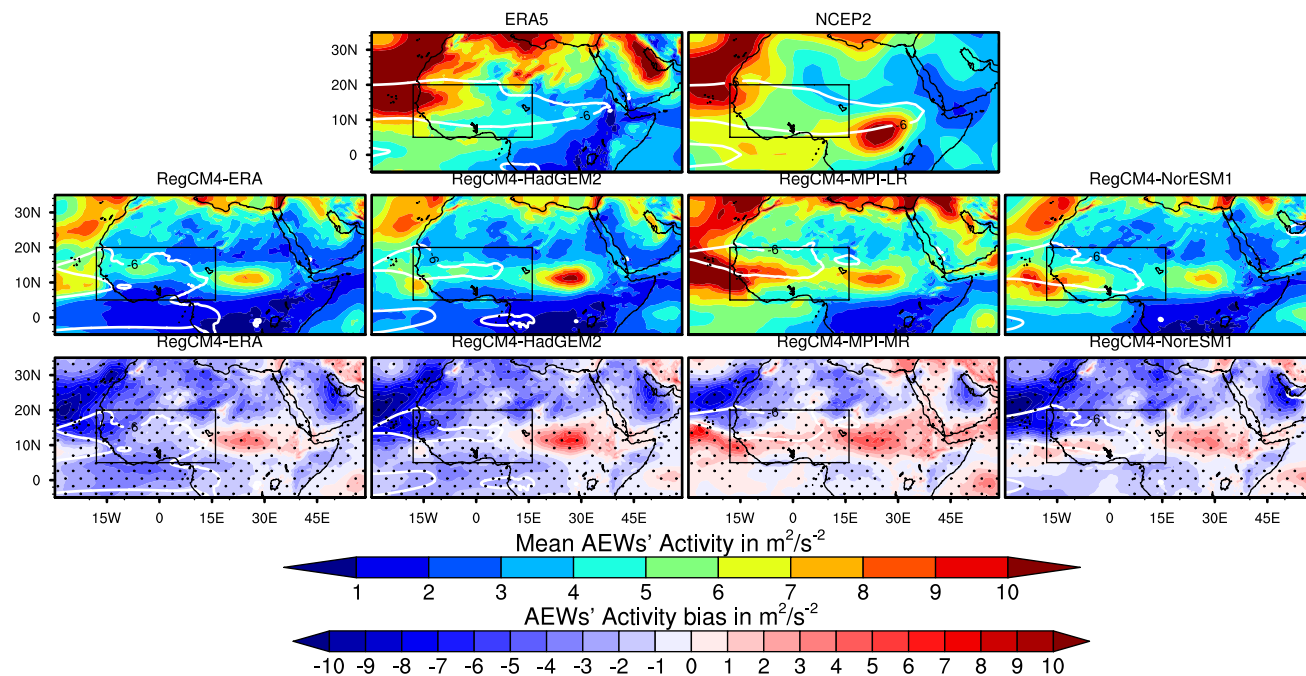

Fig. 10 Mean (1980–2005) seasonal climatology of the variance (in $m^2 \cdot s^{-2}$) of the 2–10 day passband filtered 700 hPa daily meridional component of the wind (v-wind) (1st and 2nd rows) and variance bias (3rd row). The climatology is obtained from reanalysis data (ERA5 and NCEP2) and from RegCM4-v7 experiments. The biases are computed relative to ERA5 reanalysis, from RegCM4-v7 experiments. Daily v-wind data are not available for REMO2015. The stippling occurs where the difference between the dataset under consideration and the ERA5 reanalysis dataset is statistically significant at the 95% confidence level by means of the Student's t-test. The white contour in each plot denotes the 6 m·s^{-1} zonal wind contour, averaged between 700–600 hPa and is indicative of the mean location of the AEJ core

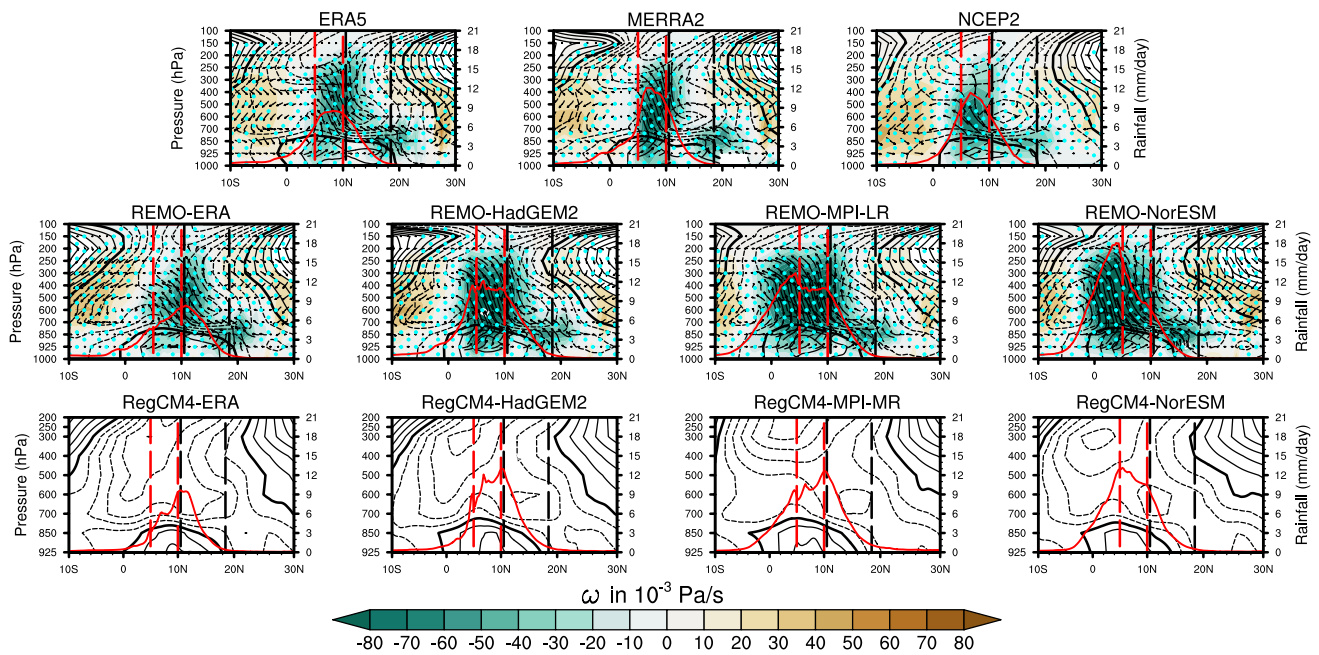**Fig. 11** Height-latitude cross-section of the vertical velocity (ω in Pa.s⁻¹; shaded), the vertical motion of meridional wind and ω (vectors), and the monthly precipitation (mm/day; red lines). Data used are from ERA5, MERRA-2 and NCEP2 reanalysis data, and from the REMO2015 and RegCM4-v7 experiments over the period 1980–2005. The vertical velocity data are not available for RegCM4-v7

experiments. As the units are Pa.s⁻¹, negative values of omega means upward motions. The stippling indicates the grid points where the difference between the dataset under consideration and the ensemble mean of the three reanalysis products is statistically significant at the 95% confidence level using the Student's *t*-test

rainfall biases, which corroborate the aforementioned findings suggesting biases in the simulated AEJ as the main drivers of models' wetness or dryness over the Sahel. In fact, when a model simulates stronger AEWs' activity, it also overestimates rainfall (e.g. RegCM4-MPI-MR). Conversely, the simulation of weaker AEWs' activity results in less precipitation, especially over the Sahel (e.g. RegCM4-ERA, RegCM4-HadGEM2 and RegCM4-NorESM1). The AEWs' troughs are linked to a cyclonic convective circulation in the lower and middle layers of the troposphere. Thus, an underestimated (overestimated) AEWs' activity leads to a weak (strong) southwesterly flow and thereby a weak (strong) moisture transport to feed MCSs embedded within the AEJ (Dieng et al. 2014). We previously showed that REMO2015 experiments better represent the AEJ than RegCM4-v7 experiments (Fig. 9). This would likely suggest that REMO2015 experiments also better represent AEWs than those of RegCM4-v7, although the two RCMs have simulated a weaker AEJ-AEWs (compared to reanalyses) complex system, especially for RegCM4-v7. AEWs being the main mechanism controlling the convection over WA (Diedhiou et al. 1999), the presence of biases in AEWs may indicate biases in simulated convection.

Finally, Fig. 11 shows how convection responds to different regional atmospheric circulation. It should be noted that the term convection here refers

to the wind ascent motions because, in CORDEX-CORE RCMs, the convection is parameterized and not explicitly resolved. As vertical velocity is not available from RegCM4, the analysis is presented for REMO2015 only. Results show that precipitation dry biases over the Sahel in reanalyses are linked to shallow ascents; reversely over the Guinea Coast, rainfall wet biases are results of deep convection. Also in RCM experiments, rainfall dry and wet biases are associated with shallow and deep-ascent motions, respectively. This corroborates the aforementioned findings on the way simulated atmospheric circulations modulate the convection through the variability in the moisture availability.

To understand the reasons for the convection bias in more detail we explored the modeled vertical structure of moist static energy (*h,* Fig. 12) and equivalent potential temperature (θ$_e$, Fig. 13). The moist static energy helps understanding how the large-scale tropical circulation interacts with the regional atmospheric moisture column, thus providing a comprehensive evaluation of how well RCMs simulate these tropical disturbances (stability/instability) that initiate convection. Results show that the way biases in modeled atmospheric stability/instability are associated with convection biases (Fig. 11) differs from one RCM
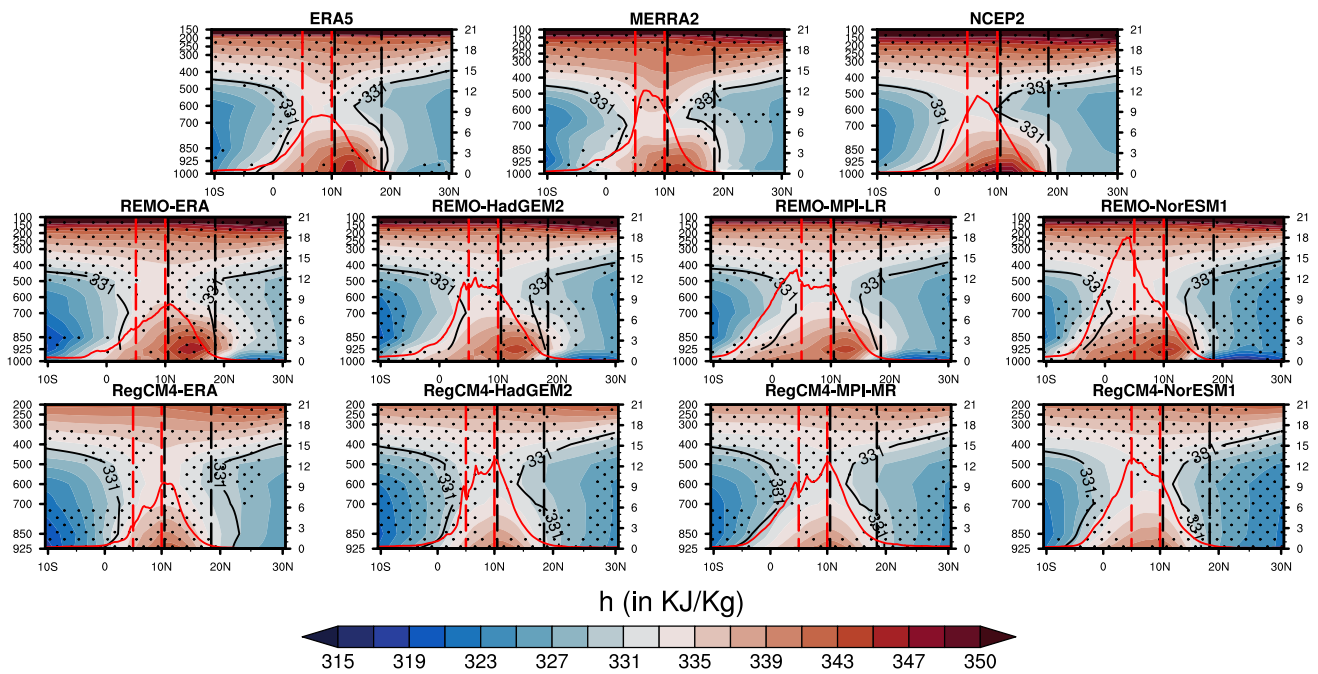
Fig. 12 Latitude-height cross-sections of the moist static energy (*h*; kJ.kg^{-1}). Data used are from reanalysis data (ERA5, MERRA-2, and NCEP2) and from the REMO2015 and RegCM4-v7 experiments over the period 1980–2005. The 331-K contour of the equivalent potential temperature (θ_e; black line) highlights the convection band. The red lines are the latitudinal migration of the rainband (mm.day^{-1}). The stippling occurs where the difference between the dataset under consideration and the ensemble mean of the three reanalysis products is statistically significant at the 95% confidence level by means of the Student's *t*-test
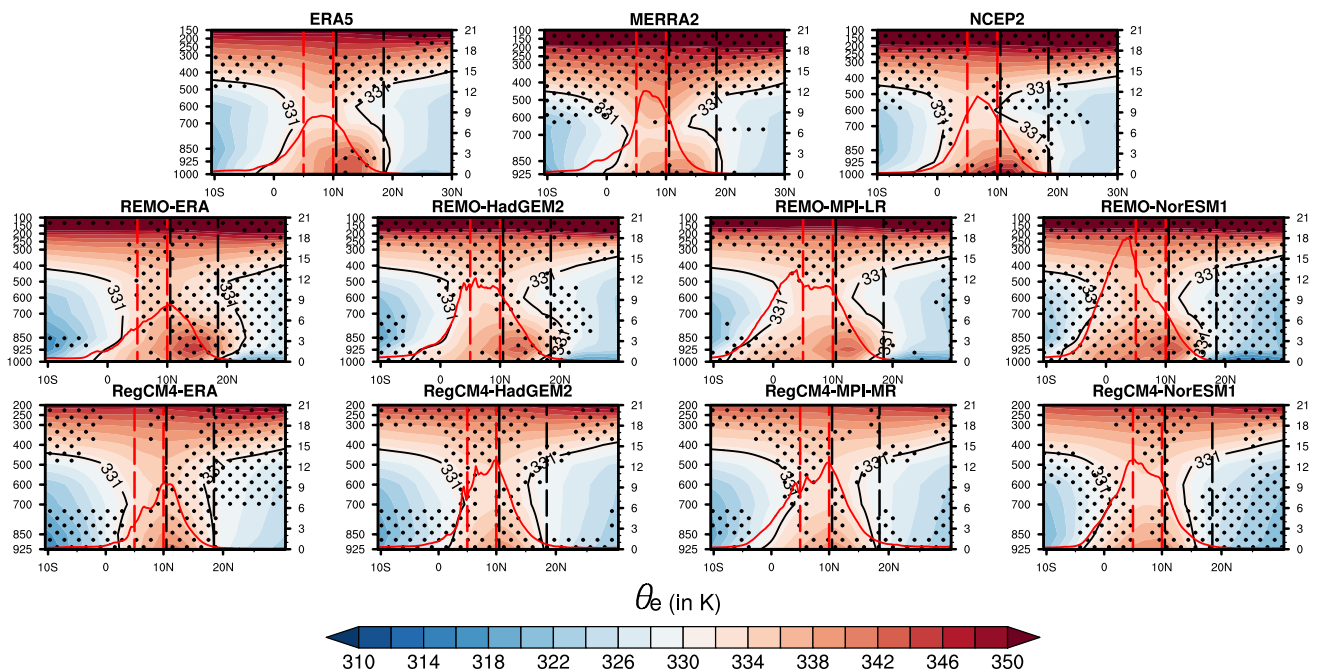

Fig. 13 Latitude-height cross-sections of the equivalent potential temperature (θ_e in K). Data used are from reanalysis data (ERA5, MERRA-2, and NCEP2) and from the REMO2015 and RegCM4-v7 experiments over the period 1980–2005. The 331-K contour shows the convection band. The red lines are the latitudinal migration of the rainband (mm.day^{-1}). The stippling occurs where the difference between the dataset under consideration and the ensemble mean of the three reanalysis products is statistically significant at the 95% confidence level by means of the Student's *t*-test

run to another. This process would be also different from what is observed in reanalyses. For instance, all reanalysis products feature precipitation dry biases over the Sahel (Fig. 1): however, they feature high values of both h (Fig. 12) and θ_e (especially ERA5 and NCEP2; see Fig. 13) in the lower layers of the atmosphere, a sign of strong disturbances, which should lead to deep convection. However, all reanalysis datasets show shallow convection over the Sahel (Fig. 11). On the other hand, some RCMs (REMO-ERA, REMO-HadGEM2, REMO-MPI-LR) do simulate deep convection over the Sahel (Fig. 11) and high values of h and θ_e in the bottom layers (Figs. 12 and 13), a sign of strong atmospheric instability, but they overestimate precipitation over the region (Fig. 1). Finally, as suggested by Grist and Nicholson (2001) and Nicholson and Grist (2003), modeled convection over the Sahel may be influenced by dynamic factors (AEJ in mid-tropospheric layers) rather than thermodynamic ones. Our results indicate a need for further investigation of the relationship between atmospheric instability, convection and precipitation in both reanalysis and climate models.

6 Conclusions and discussion

In this study, we investigated the performances of two new generation high resolution, (~ 25 km) CORDEX-CORE RCMs in simulating observed precipitation over West Africa during the monsoon season (JAS). The rainfall biases are analyzed and the physical underlying processes associated with these biases are examined to understand how well the models represent the WAM system. Drivers of the WAM system used for the models' diagnostic include land-ocean feedback processes via SST, land surface temperature, MSLP, land surface pressure variability and evaporation; the regional atmospheric circulation such as the AEJ, AEWs, TEJ, WAWJ and finally convection and associated thermodynamic (h and θ_e) factors. Some RCM experiments show a north (negative/positive)-south (positive/negative) dipole-like rainfall bias, while others simulate positive or negative rainfall biases over the majority of WA. In this study, we found that the following physical mechanisms are potential drivers of precipitation biases across simulations:

1. Most GCM driven RCMs overestimate SST (which is inherited from the driving GCM) over the whole of the Guinea Gulf. Enhanced SST increases moisture availability through enhanced evaporation. However, RCMs show weaker MSLP over the eastern Atlantic Ocean, including the South Atlantic High-pressure system in

part or in full, which can result in too little moisture advection from the ocean towards the Guinea Gulf. Inland, surface pressures are also slightly underestimated including African thermal lows, but this does not alter models' precipitation biases owing to the lack of involvement of lows' pressure systems in the atmospheric circulation anomalies.

2. Biases in the modeled land-ocean temperature and pressure contrasts (∇T and ∇P) also induce biases in the simulated monsoon flux strength, leading to modifications in the latitudinal positioning of the monsoon convective system. Indeed, simulations that show rainfall wet biases over the Sahel also feature moisture being advected further inland, compared to those representing dry biases over the same area. Specifically, strong (weak) ∇T and ∇P induce more moisture to be advected over the Sahel (Guinea Coast) through southeasterlies recurving into southwesterlies and via the West African westerly jet (WAWJ).

3. The AEJ plays an important role in models' rainfall biases, especially over the Sahel: indeed, RCM simulations that feature precipitation dry biases over the Sahel, simulate an equatorward shifting of the AEJ, promoting strong moisture divergence from the region, thereby drying mid-tropospheric layers and suppressing convection. Contrastingly, simulations with precipitation wet biases over the same domain exhibit a poleward (northward) shifting and weaker AEJ, conditions that favor important amounts of moisture convergence into the region, therefore moistening mid-tropospheric layers and increasing convection. These results adequately corroborate the known rainfall-AEJ coupling process over the Sahel (Nicholson and Grist 2003; Bercos-Hickey and Patricola 2021). Although rainfall biases are interpreted here as being induced by that of related AEJ, the reverse may be also true, owing to feedback in processes. Bercos-Hickey et al. (2020) showed that the Saharan mineral dust and the West African precipitation feedback on the AEJ by modifying the meridional temperature gradient over North Africa.

4. Biases in the modeled AEJ induce biases in modeled AEWs with a strong implication on simulated rainfall climatology, especially over the Sahel. RCM runs that feature weaker (stronger) AEJ also model weaker (stronger) AEWs' activity leading to dry (wet) rainfall biases. This result reveals a lack of coupling between AEWs and rainfall, and is consistent with previous findings by Skinner and Diffenbaugh (2013) using CMIP3 GCMs. They showed that the force of modeled AEWs' activity is strongly dependent on the simulated intensity and positioning of the AEJ and low-level westerlies. The cyclonic convective circulation has likely weakened

because of the underestimating strength of the AEJ and the subsequent AEWs' activity.

5. Over the Sahel, rainfall dry biases in the RCMs are associated with shallow ascent motions, whereas wet biases to deep-ascent motions. However, the way the moist static energy (h) and equivalent potential temperature (θ_e) are associated with convection differs between reanalyses and RCM experiments, and from one RCM run to another. We found that over the Sahel, strong h and θ_e values are related to moist convection in some RCM experiments (e.g. REMO-ERA, REMO-HadGEM2, REMO-MPI-LR, RegCM4-MPI-MR), whereas the same conditions drive, instead, dry convection in reanalyses. Also, REMO-NorESM1 which features precipitation dry biases over the Sahel shows rather high values of h and θ_e in the lower atmospheric layers, a condition of atmospheric instability that should induce convection and therefore moistening the region.

Numerous studies have demonstrated the strong influence of large-scale processes on the WAM system, for instance, the Pacific Decadal Oscillation, the El Niño-Southern Oscillation or the North Atlantic Oscillation (Zhang and Zhou 2011; Diatta and Fink 2014). These factors are not investigated in the present study although their representation in the driving GCMs might have a strong impact on the RCMs' rainfall biases. This suggests that the current work is far from exhaustive in terms of the sources of precipitation biases in CORDEX-CORE RCMs. Also, here (and in addition to other studies, e.g. Dosio et al. 2021a; Tamoffo et al. 2021), it is shown that there are still important rainfall biases in the results of the dynamical downscaling conducted with CORDEX-CORE RCMs over Africa, even if the horizontal resolution is twice that of the original CORDEX simulations. Although increasing models' resolution is proven to be beneficial where regional- and local-scale processes play an important role in a region's climate, it is not sufficient to overcome many model deficiencies (Doblas-Reyes et al. 2021). Wu et al. (2020) demonstrated the dominance effect of the model's physics parameterization over the resolution on precipitation climatology across Africa. They showed that the model physics controls the spatial pattern of seasonal rainfall biases while the resolution mainly influences the precipitation intensity, thereby suggesting the necessity of models' formulation for a better representation of the climate. The manner models are configured could also be an important source of uncertainties, for instance, when the convection is parameterized instead to be explicitly resolved; or when RCMs are not coupled with an ocean model, in order to physically modify SST prescribed by driving GCMs. In the first case, promising results are becoming available from convection-permitting models (CPM), i.e. RCMs run at very high resolution (around

5 km or less) so that convection can be explicitly simulated. These simulations showed significant improvements in small-scale precipitation characteristics (such as intensity and diurnal cycle) and notable effects on projected changes in extremes. However, given the significant amount of computational resources involved in the simulations, results are available only for a very limited period of time (10 years or less) (Kendon et al. 2019; Kouadio et al. 2020; Senior et al. 2021). In the second case, the RCM community has started to develop models that incorporate more components of the climate system, like regional oceans, or biogeochemistry (Doblas-Reyes et al. 2021). However, the majority of dynamical downscaling using RCMs is still done with SST prescribed by the driving GCM. This was indeed part of the CORDEX protocol. Nevertheless, the results of the downscaling employed in this paper capture well the basic features of the WAM system, as most of the analyzed physical underlying processes confirm the reasonableness of the simulated monsoon rainfall climatology.

Finally, as mentioned, the direct comparison of present and future climate as simulated by RCMs and GCMs has been performed in several previous studies (see e.g. Dosio et al. 2021a and reference within), including the analysis of the added value of downscaling (e.g. Dosio et al. 2015; Gibba et al. 2019). However, the quantification of added value by means of a specific, thorough process-based analysis of the performances of the RCMs compared to those of the driving GCMs is still missing (see e.g. discussion in Dosio et al. 2019) but outside the scope of this particular work (which focuses on the performances of RCMs only), and is left for future research.

developed by NASA, is available online (at https://disc.gsfc.nasa.gov/datasets?keywords1/4%22MERRA-2%22&page1/41&source1/4Models%2FAnalyses%20MERRA-2). NCEP2 data set is provided by the NOAA/OAR/ESRL PSD and is available through the website https://psl.noaa.gov/data/gridded/data.ncep.reanalysis2.html.

The GPCC observational data set is available at https://opendata.dwd.de/climate_environment/GPCC/html/fulldata-monthly_v2020_doi_download.html. The GPCP-v2.3 combined precipitation data set is available at https://www.esrl.noaa.gov/psd/data/gridded/data.gpcp.html; the CRU-v4.04 dataset is available at https://data.ceda.ac.uk/badc/cru/data/cru_ts/cru_ts_4.04/data/pre (UEA, 2019); The UDel-4.01 data set is available at http://climate.geog.udel.edu/~climate/html_pages/download.html (University of Delaware, 2019);

The CHIRPS2 data are available at https://data.chc.ucsb.edu/products/CHIRPS-2.0/global_daily/netcdf/.

The corresponding author is available for providing NIC131 data upon request.

ARC2 data are available at http://iridl.ldeo.columbia.edu/SOURCES/.NOAA/.NCEP/.CPC/.FEWS/.Africa/.DAILY/.ARC2/.daily/.

The UGDP is available at https://psl.noaa.gov/data/gridded/data.cpc.globalprecip.html.

The HadISST SST data are available at https://www.metoffice.gov.uk/hadobs/hadisst/data/download.html.

The ERSST-v5 SST data are available at https://psl.noaa.gov/data/gridded/data.noaa.ersst.v5.html.

Declarations

Competing interests Not applicable.

References

Akinsanola AA, Zhou W (2018) Dynamic and thermodynamic factors controlling increasing summer monsoon rainfall over the west African Sahel. Clim Dyn 52(7–8):4501–4514. https://doi.org/10.1007/s00382-018-4394-x

Akinsanola AA, Ogunjobi KO, Gbode IE, Ajayi VO (2015) Assessing the capabilities of three regional climate models over CORDEX Africa in simulating west African summer monsoon precipitation. Adv Meteorol 2015:1–13. https://doi.org/10.1155/2015/935431

Akinsanola AA, Ogunjobi KO, Ajayi VO, Adefisan EA, Omotosho JA, Sanogo S (2016) Comparison of five gridded precipitation products at climatological scales over west Africa. Meteorol Atmos Phys 129(6):669–689. https://doi.org/10.1007/s00703-016-0493-6

Akinsanola AA, Ajayi VO, Adejare AT, Adeyeri OE, Gbode IE, Ogunjobi KO, Nikulin G, Abolude AT (2017) Evaluation of rainfall simulations over west Africa in dynamically downscaled CMIP5 global circulation models. Theor Appl Climatol. https://doi.org/10.1007/s00704-017-2087-8

Ashfaq M, Cavazos T, Reboita MS, Torres-Alavez JA, Im E, Olusegun CF, Giorgi F (2020) Robust late twenty-first century shift in the regional monsoons in RegCM-CORDEX simulations. Clim Dyn 57(5–6):1463–1488. https://doi.org/10.1007/s00382-020-05306-2

Balas N, Nicholson SE, Klotter D (2007) The relationship of rainfall variability in West Central Africa to sea-surface temperature fluctuations. Int J Clim 27(10):1335–1349. https://doi.org/10.1002/joc.1456

Bentsen M, Bethke I, Debernard JB, Iversen T, Kirkevåg A, Seland Ø, Kristjánsson JE (2013) The Norwegian earth system model, NorESM1-M – part 1: description and basic evaluation of the physical climate. Geosci Model Dev 6(3):687–720. https://doi.org/10.5194/gmd-6-687-2013

Bercos-Hickey E, Patricola CM (2021) Anthropogenic influences on the African easterly jet–African easterly wave system. Clim Dyn 57(9–10):2779–2792. https://doi.org/10.1007/s00382-021-05838-1

Bercos-Hickey E, Nathan TR, Chen S-H (2020) On the relationship between the African easterly jet, Saharan mineral dust aerosols, and west African precipitation. J Clim 33(9):3533–3546. https://doi.org/10.1175/jcli-d-18-0661.1

Biasutti M (2013) Forced Sahel rainfall trends in the CMIP5 archive. J Geophys Res Atmos 118:1613–1623. https://doi.org/10.1002/jgrd.50206

Birch CE, Parker D, Marsham J, Copsey D, Garcia-Carreras L (2014) A seamless assessment of the role of convection in the water cycle of the west African monsoon. J Geophys Res Atmos 119(6):2890–2912. https://doi.org/10.1002/2013JD020887

Boone AA, Poccard-Leclercq I, Xue Y et al (2010) Evaluation of the WAMME model surface fluxes using results from the AMMA land-surface model intercomparison project. Clim Dyn 35:127–142. https://doi.org/10.1007/s00382-009-0653-1

Cadet DL, Nnoli NO (2007) Water vapour transport over Africa and the Atlantic ocean during summer 1979. Q J R Meteorol Soc 113(476):581–602. https://doi.org/10.1002/qj.49711347609

Clark DB, Xue Y, Harding RJ, Valdes PJ (2001) Modeling the impact of land surface degradation on the climate of tropical north Africa. J Clim 14(8):1809–1822. https://doi.org/10.1175/1520-0442(2001)0142.0.co;2

Collins WJ, Bellouin N, Doutriaux-Boucher M, Gedney N, Halloran P, Hinton T, Woodward S (2011) Development and evaluation of an earth-system model – HadGEM2. Geosci Model Dev 4(4):1051–1075. https://doi.org/10.5194/gmd-4-1051-2011

Cook KH (1999) Generation of the african easterly jet and its role in determining west African precipitation. J Clim 12(5):1165–1184

Cook KH, Vizy EK (2006) Coupled model simulations of the west African monsoon system: twentieth- and twenty-first-century simulations. J Clim 19(15):3681–3703. https://doi.org/10.1175/jcli3814.1

Coppola E, Raffaele F, Giorgi F, Giuliani G, Xuejie G, Ciarlo JM, Sines TR, Torres-Alavez JA, Das S, di Sante F, Pichelli E, Glazer R, Müller SK, Abba Omar S, Ashfaq M, Bukovsky M, Im E-S, Jacob D, Teichmann C et al (2021) Climate hazard indices projections based on CORDEX-CORE, CMIP5 and CMIP6 ensemble. Clim Dyn. https://doi.org/10.1007/s00382-021-05640-z

Dee DP, Uppala SM, Simmons AJ, Berrisford P, Poli P, Kobayashi S et al (2011) The ERA-Interim reanalysis: configuration and performance of the data assimilation system. Q J R Meteorol Soc 137(656):553–597. https://doi.org/10.1002/qj.828

Diallo I, Sylla MB, Giorgi F, Gaye AT, Camara M (2012) Multimodel GCM-RCM ensemble-based projections of temperature and precipitation over west Africa for the early 21st century. Int J Geophys 2012:1–19. https://doi.org/10.1155/2012/972896

Diallo I, Bain CL, Gaye AT, Moufouma-Okia W, Niang C, Dieng MDB, Graham R (2014) Simulation of the west African monsoon onset using the HadGEM3-RA regional climate model. Clim Dyn 43(3–4):575–594. https://doi.org/10.1007/s00382-014-2219-0

Diallo I, Giorgi F, Sukumaran S, Stordal F, Giuliani G (2015) Evaluation of RegCM4 driven by CAM4 over southern Africa: mean climatology, interannual variability and daily extremes of wet season temperature and precipitation. Theor Appl Climatol. https://doi.org/10.1007/s00704-014-1260-6

Diallo I, Giorgi F, Deme A, Tall M, Mariotti L, Gaye AT (2016) Projected changes of summer monsoon extremes and hydroclimatic

regimes over west Africa for the twenty-first century. Clim Dyn 47(12):3931–3954. https://doi.org/10.1007/s00382-016-3052-4

Diatta S, Fink AH (2014) Statistical relationship between remote climate indices and west African monsoon variability. Int J Climatol 34:3348–3367. https://doi.org/10.1002/joc.3912

Diedhiou A, Janicot S, Viltard A, de Felice P (1998) Evidence of two regimes of easterly waves over west Africa and the tropical Atlantic. Geophys Res Lett 25(15):2805–2808. https://doi.org/10.1029/98gl02152

Diedhiou A, Janicot S, Viltard A, de Felice P, Laurent H (1999) Easterly wave regimes and associated convection over west Africa and tropical Atlantic: results from the NCEP/NCAR and ECMWF reanalyses. Clim Dyn 15(11):795–822. https://doi.org/10.1007/s003820050316

Dieng AL, Eymard L, Sall SM, Lazar A, Leduc-Leballeur M (2014) Analysis of strengthening and dissipating mesoscale convective systems propagating off the west African coast. Mon Weather Rev 142(12):4600–4623. https://doi.org/10.1175/mwr-d-13-00388.1

Dieng D, Smiatek G, Bliefernicht J, Heinzeller D, Sarr A, Gaye AT, Kunstmann H (2017) Evaluation of the COSMO-CLM high-resolution climate simulations over west Africa. J Geophys Res: Atmos 122(3):1437–1455. https://doi.org/10.1002/2016jd025457

Doblas-Reyes, F.J., A.A. Sörensson, M. Almazroui, A. Dosio, W.J. Gutowski, R. Haarsma, R. Hamdi, B. Hewitson, W.-T. Kwon, B.L. Lamptey, D. Maraun, T.S. Stephenson, I. Takayabu, L. Terray, A. Turner, and Z. Zuo, (2021): Linking Global to Regional Climate Change. In: Climate Change 2021: The Physical Science Basis. Contribution of Working Group I to the Sixth Assessment Report of the Intergovernmental Panel on Climate Change. Masson-Delmotte, V., P. Zhai, A. Pirani, S.L. Connors, C. Péan, S. Berger, N. Caud, Y. Chen, L. Goldfarb, M.I. Gomis, M. Huang, K. Leitzell, E. Lonnoy, J.B.R. Matthews, T.K. Maycock, T. Waterfield, O. Yelekçi, R. Yu, and B. Zhou (eds.). Cambridge University Press

Dosio A, Panitz HJ (2016) Climate change projections for CORDEX-Africa with COSMO-CLM regional climate model and differences with the driving global climate models. Clim Dyn 46(5):1599–1625. https://doi.org/10.1007/s00382-015-2664-4

Dosio A, Panitz H-J, Schubert-Frisius M, Lüthi D (2015) Dynamical downscaling of CMIP5 global circulation models over CORDEX-Africa with COSMO-CLM: evaluation over the present climate and analysis of the added value. Clim Dyn 44(9–10):2637–2661. https://doi.org/10.1007/s00382-014-2262-x

Dosio A, Jones R, Jack C, Lennard C, Nikulin G, Hewitson B (2019) What can we know about future precipitation in Africa? Robustness, significance and added value of a large ensemble of regional climate models. Clim Dyn. https://doi.org/10.1007/s00382-019-04900-3

Dosio A, Turner AG, Tamoffo AT, Sylla MB, Lennard C, Jones RG et al (2020) A tale of two futures: contrasting scenarios of future precipitation for west Africa from an ensemble of regional climate models. Environ Res Lett 15:064007. https://doi.org/10.1088/1748-9326/ab7fde

Dosio A, Jury MW, Almazroui M, Ashfaq M, Diallo I, Engelbrecht FA, Tamoffo AT (2021a) Projected future daily characteristics of African precipitation based on global (CMIP5, CMIP6) and regional (CORDEX, CORDEX-CORE) climate models. Clim Dyn 57(11–12):3135–3158. https://doi.org/10.1007/s00382-021-05859-w

Dosio A, Pinto I, Lennard C, Sylla MB, Jack C, Nikulin G (2021b) What can we know about recent past precipitation over Africa daily characteristics of African precipitation from a large ensemble of observational products for model evaluation. Earth Sp Sci. https://doi.org/10.1029/2020EA001466

Druyan LM, Feng J, Cook KH et al (2010) The WAMME regional model intercomparison study. Clim Dyn 35:175–192. https://doi.org/10.1007/s00382-009-0676-7

Fink AH, Reiner A (2003) Spatiotemporal variability of the relation between African easterly waves and west African squall lines in 1998 and 1999. J Geophys Res. https://doi.org/10.1029/2002jd002816

Fotso-Nguemo TC, Vondou DA, Pokam WM, Djomou ZY, Diallo I, Haensler A, Tchawoua C (2017) On the added value of the regional climate model REMO in the assessment of climate change signal over central Africa. Clim Dyn 49:3813–3838. https://doi.org/10.1007/s00382-017-3547-7

Funk Chris et al (2015) The climate hazards infrared precipitation with stations—a new environmental record for monitoring extremes. Sci Data. https://doi.org/10.1038/sdata.2015.66

Gibba P, Sylla MB, Okogbue EC, Gaye AT, Nikiema M, Kebe I (2019) State-of-the-art climate modeling of extreme precipitation over Africa: analysis of CORDEX added-value over CMIP5. Theor Appl Climatol 137(1–2):1041–1057. https://doi.org/10.1007/s00704-018-2650-y

Giorgi F, Gutowski WJ (2015) Regional dynamical downscaling and the CORDEX initiative. Annu Rev Environ Resour 40(1):467–490. https://doi.org/10.1146/annurev-environ-102014-021217

Giorgi F, Jones C, Asrar GR et al (2009) Addressing climate information needs at the regional level: the CORDEX framework. World Meteorol Org (WMO) Bull 58(3):175

Giorgi F, Coppola E, Solmon F, Mariotti L, Sylla M, Bi X, Brankovic C (2012) RegCM4: model description and preliminary tests over multiple CORDEX domains. Clim Res 52:7–29. https://doi.org/10.3354/cr01018

Giorgi F, Coppola E, Teichmann C, Jacob D (2021) Editorial for the CORDEX-CORE experiment I special issue. Clim Dyn. https://doi.org/10.1007/s00382-021-05902-w

Gnitou GT, Tan G, Niu R, Nooni IK (2021) Assessing past climate biases and the added value of CORDEX-CORE precipitation simulations over Africa. Remote Sens 13(11):2058. https://doi.org/10.3390/rs13112058

Grist JP, Nicholson SE (2001) A study of the dynamic factors influencing the rainfall variability in the west African Sahel. J Clim 14(7):1337–1359. https://doi.org/10.1175/1520-0442(2001)0142.0.co;2

Gutowski WJ et al (2016) WCRP coordinated regional downscaling experiment (CORDEX): a diagnostic MIP for CMIP6. Geosci Model Dev 9:4087–4095. https://doi.org/10.5194/gmd-9-4087-2016

Harris I, Osborn TJ, Jones P, Lister D (2020) Version 4 of the CRU TS monthly high-resolution gridded multivariate climate dataset. Sci Data 7(1):109. https://doi.org/10.1038/s41597-020-0453-3

Hersbach H, Bell B, Berrisford P et al (2020) The ERA5 global reanalysis. Q J R Meteorol Soc. https://doi.org/10.1002/qj.3803

Holtslag AAM, De Bruijn EIF, Pan HL (1990) A high resolution air mass transformation model for short-range weather forecasting. Mon Weather Rev 118(8):1561–1575. https://doi.org/10.1175/1520-0493(1990)118<1561:AHRAMT>2.0.CO;2

Huang B, Thorne PW, Banzon VF, Boyer T, Chepurin G, Lawrimore JH, Zhang H (2017) Extended reconstructed sea surface temperature, version 5 (ERSSTv5): upgrades, validations, and intercomparisons. J Clim 30(20):8179–8205. https://doi.org/10.1175/jcli-d-16-0836.1

Huffman GJ, Adler RF, Bolvin DT, Gu G (2009) Improving the global precipitation record: GPCP version 2.1. Geophys Res Lett. https://doi.org/10.1029/2009GL040000

Ilori OW, Balogun IA (2021) Evaluating the performance of new CORDEX-Africa regional climate models in simulating west African rainfall. Model Earth Syst Environ. https://doi.org/10.1007/s40808-021-01084-w

Jacob D (2001) A note to the simulation of the annual and interannual variability of the water budget over the Baltic Sea drainage basin. Meteor Atmos Phys 77:61–73. https://doi.org/10.1007/s007030170017

Jacob D, Podzun R (1997) Sensitivity studies with the regional climate model REMO. Meteor Atmos Phys 63:119–129. https://doi.org/10.1007/bf01025368

Jacob D, Elizalde A, Haensler A, Hagemann S, Kumar P, Podzun R, Rechid D, Remedio AR, Saeed F, Sieck K, Teichmann C, Wilhelm C (2012) Assessing the transferability of the regional climate model REMO to Different COordinated Regional Climate Downscaling EXperiment (CORDEX) Regions. Atmosphere 3(4):181–199. https://doi.org/10.3390/atmos3010181

James R, Washington R, Jones R (2015) Process-based assessment of an ensemble of climate projections for west Africa. J Geophys Res Atmos 120:1221–1238. https://doi.org/10.1002/2014JD022513

James R, Washington R, Abiodun B, Kay G, Mutemi J, Pokam W, Senior C (2018) Evaluating climate models with an African Lens. Bull Am Meteor Soc 99(2):313–336. https://doi.org/10.1175/bams-d-16-0090.1

Janowiak J, Xie P (2011) Islscp Ii Gts Gauge-based analyses of daily precipitation over global land areas. ORNL Distrib Act Arch Cent Datasets. https://doi.org/10.3334/ornldaac/1001

Kamga AF, Jenkins GS, Gaye AT, Garba A, Sarr A, Adedoyin A (2005) Evaluating the national center for atmospheric research climate system model over west Africa: present-day and the 21st century A1 scenario. J Geophys Res 110:D03106. https://doi.org/10.1029/2004JD004689

Kanamitsu M, Yoshimura K, Yhang Y, Hong S (2010) Errors of interannual variability and trend in dynamical downscaling of reanalysis. J Geophys Res 115:D17115. https://doi.org/10.1029/2009jd013511

Kendon EJ, Stratton RA, Tucker S, Marsham JH, Berthou S, Rowell DP, Senior CA (2019) Enhanced future changes in wet and dry extremes over Africa at convection-permitting scale. Nat Commun 10(1):1794. https://doi.org/10.1038/s41467-019-09776-9

Klutse NAB, Sylla MB, Diallo I, Sarr A, Dosio A, Diedhiou A, Kamga A, Lamptey B, Ali A, Gbobaniyi EO, Owusu K, Lennard C, Hewitson B, Nikulin G, Panitz HJ, Büchner M (2016) Daily characteristics of west African summer monsoon precipitation in CORDEX simulations. Theor Appl Climatol. https://doi.org/10.1007/s00704-014-1352-3

Koster RD, Dirmeyer PA, Guo Z, Bonan G, Chan E, Cox P, Gordon CT, Kanae S, Kowalczyk E, Lawrence D, Liu P, Lu CH, Malyshev S, McAvaney B, Mitchell K, Mocko D, Oki T, Oleson K, Pitman A, Sud YC, Taylor CM, Verseghy D, Vasic R, Xue Y, Yamada T (2004) Regions of strong coupling between soil moisture and precipitation. Science. 305(5687):1138–1140. https://doi.org/10.1126/science.1100217

Kouadio K, Bastin S, Konare A, Ajayi VO (2020) Does convection-permitting simulate better rainfall distribution and extreme over Guinean coast and surroundings? Clim Dyn 55(1–2):153–174. https://doi.org/10.1007/s00382-018-4308-y

Lebel T, Diedhiou A, Laurent H (2003) Seasonal cycle and interannual variability of the Sahelian rainfall at hydrological scales. J Geophys Res 108(D8):8389. https://doi.org/10.1029/2001JD001580

Legates DR, Willmott CJ (1990) Mean seasonal and spatial variability in gauge-corrected, global precipitation. Int J Climatol 10(2):111–127. https://doi.org/10.1002/joc.3370100202

Leroux S, Hall NMJ (2009) On the relationship between African easterly waves and the African easterly jet. J Atmos Sci 66:2303–2316. https://doi.org/10.1175/2009JAS2988.1

Lohmann U, Roeckner E (1996) Design and performance of a new cloud microphysics scheme developed for the ECHAM4 general circulation model. Clim Dyn 12:557–572

Louis JF (1979) A parametric model of vertical eddy fluxes in the atmosphere. Bound Layer Meteorol 17(2):187–202

Maidment RI, Allan RP, Black E (2015) Recent observed and simulated changes in precipitation over Africa. Geophys Res Lett 42(19):8155–8164. https://doi.org/10.1002/2015GL065765

Marcella MP, Eltahir EAB (2014) The role of mineral aerosols in shaping the regional climate of west Africa. J Geophys Res 119:1–14. https://doi.org/10.1002/2012JD019394

Mariotti L, Diallo I, Coppola E, Giorgi F (2014) Seasonal and intraseasonal changes of African monsoon climates in 21st century CORDEX projections. Clim Change 125(1):53–65. https://doi.org/10.1007/s10584-014-1097-0

Martin ER, Thorncroft CD (2013) The impact of the AMO on the west African monsoon annual cycle. Q J R Meteorol Soc 140(678):31–46. https://doi.org/10.1002/qj.2107

Meehl GA, Covey C, Taylor KE, Delworth T, Stouffer RJ, Latif M, McAvaney B, Mitchell JFB (2007) The WCRP CMIP3 multi-model dataset: a new era in climate change research. Bull Am Meteorol Soc 88(9):1383–1394

Monerie PA, Fontaine B, Roucou P (2012) Expected future changes in the African monsoon between 2030 and 2070 using some CMIP3 and CMIP5 models under a medium-low RCP scenario. J Geophys Res Atmos 117:D16111. https://doi.org/10.1029/2012JD017510

Monerie P-A, Robson JI, Dunstone NJ, Turner AG (2021) Skilful seasonal predictions of global monsoon summer precipitation with DePreSys3. Environ Res Lett 16(10):104035. https://doi.org/10.1088/1748-9326/ac2a65

N'Datchoh ET, Diallo I, Konaré A, Silué S, Ogunjobi KO, Diedhiou A, Doumbia M (2018) Dust induced changes on the West African summer monsoon features. Int J Climatol 38:452–466. https://doi.org/10.1002/joc.5187

NASA (2016). Modern-Era Retrospective analysis for Research and Applications, version 2. Goddard Earth Sciences Data and Information Services Center, accessed 12 September 2017. https://disc.gsfc.nasa.gov/daac-bin/FTPSubset.pl

Newell RE, Kidson JW (1984) African mean wind changes between sahelian wet and dry periods. J Climatol 4(1):27–33. https://doi.org/10.1002/joc.3370040103

Nicholson SE, Grist JP (2003) The seasonal evolution of the atmospheric circulation over west Africa and equatorial Africa. J Clim 16:1013–1030. https://doi.org/10.1175/15200442(2003)016%3c1013:TSEOTA%3e2.0.CO;2

Nicholson SE, Klotter D (2020) The tropical easterly jet over Africa, its representation in six reanalysis products, and its association with Sahel rainfall. Int J Climatol 41(1):328–347. https://doi.org/10.1002/joc.6623

Nicholson SE, Webster PJ (2007) A physical basis for the interannual variability of rainfall in the sahel. Q J R Meteorol Soc 133(629):2065–2084. https://doi.org/10.1002/qj.104

Nicholson SE, Funk C, Fink AH (2018) Rainfall over the African continent from the 19th through the 21st century. Global Planet Change 165:114–127. https://doi.org/10.1016/j.gloplacha.2017.12.014

Nicholson SE, Klotter D, Zhou L, Hua W (2019) validation of satellite precipitation estimates over the Congo basin. J Hydrometeorol 20(4):631–656. https://doi.org/10.1175/jhm-d-18-0118.1

Nicholson, (2013) The west African Sahel: a review of recent studies on the rainfall regime and its interannual variability. ISRN Meteorol 2013:453521. https://doi.org/10.1155/2013/453521

Novella NS, Thiaw WM (2013) African rainfall climatology version 2 for famine early warning systems. J Appl Meteorol Climatol 52(3):588–606. https://doi.org/10.1175/jamc-d-11-0238.1

Odoulami RC, Akinsanola AA (2017) Recent assessment of west African summer monsoon daily rainfall trends. Weather 73(9):283–287. https://doi.org/10.1002/wea.2965

Pal JS, Small EE, Eltahir EAB (2000) Simulation of regional-scale water and energy budgets: representation of subgrid cloud and precipitation processes within regcm. J Geophys Res Atmos 105(D24):29579–29594. https://doi.org/10.1029/2000JD90041

Patricola CM, Cook KH (2007) Dynamics of the west African monsoon under mid-holocene precessional forcing: regional climate model simulations. J Clim 20(4):694–716. https://doi.org/10.1175/jcli4013.1

Patricola CM, Saravanan R, Chang P (2018) The response of Atlantic tropical cyclones to suppression of African easterly waves. Geophys Res Lett 45(1):471–479. https://doi.org/10.1002/2017gl076081

Pinto I, Lennard C, Tadross M, Hewitson B, Dosio A, Nikulin G et al (2016) Evaluation and projections of extreme precipitation over southern Africa from two CORDEX models. Clim Change 135(3–4):655–668. https://doi.org/10.1007/s10584-015-1573-1

Popke D, Stevens B, Voigt A (2013) Climate and climate change in a radiative-convective equilibrium version of ECHAM6. J Adv Model Earth Syst 5(1):1–14. https://doi.org/10.1029/2012ms000191

Pu B, Cook KH (2012) Role of the west African westerly jet in Sahel rainfall variations. J Clim 25(8):2880–2896. https://doi.org/10.1175/jcli-d-11-00394.1

Remedio AR, Teichmann C, Buntemeyer L, Sieck K, Weber T, Rechid D, Hoffmann P, Nam C, Kotova L, Jacob D (2019) Evaluation of new CORDEX simulations using an updated Köppen–Trewartha climate classification. Atmosphere 10(11):726. https://doi.org/10.3390/atmos10110726

Schneider U, Becker A, Finger P, Meyer-Christoffer A, Ziese M, Rudolf B (2013) GPCC's new land surface precipitation climatology based on quality-controlled in situ data and its role in quantifying the global water cycle. Theor Appl Climatol 115:15–40. https://doi.org/10.1007/s00704-013-0860-x

Senior CA, Marsham JH, Berthou S, Burgin LE, Folwell SS, Kendon EJ, Klein CM, Jones RG, Mittal N, Rowell DP, Tomassini L, Vischel T, Becker B, Birch CE, Crook J, Dougill AJ, Finney DL, Graham RJ, Hart NCG et al (2021) Convection permitting regional climate change simulations for understanding future climate and informing decision making in Africa. Bull Am Meteorol Soc. https://doi.org/10.1175/BAMS-D-20-0020.1

Seth A, Rauscher SA, Biasutti M, Giannini A, Camargo SJ, Rojas M (2013) CMIP5 projected changes in the annual cycle of precipitation in monsoon regions. J Clim 26:7328–7351. https://doi.org/10.1175/JCLI-D-12-00726.1

Skinner CB, Diffenbaugh NS (2013) The contribution of African easterly waves to monsoon precipitation in the CMIP3 ensemble. J Geophys Res: Atmos 118(9):3590–3609. https://doi.org/10.1002/jgrd.50363

Sørland SL, Brogli R, Pothapakula PK, Russo E, Van de Walle J, Ahrens B et al (2021) COSMO-CLM regional climate simulations in the coordinated regional climate downscaling Experiment (CORDEX) framework: a review. Geosci Model Dev 14:5125–5154. https://doi.org/10.5194/gmd-14-5125-2021

Stevens B, Giorgetta M, Esch M, Mauritsen T, Crueger T, Rast S, Roeckner E (2013) Atmospheric component of the MPI-M earth system model: ECHAM6. J Adv Modeling Earth Syst 5(2):146–172. https://doi.org/10.1002/jame.20015

Stouffer RJ, Eyring V, Meehl GA, Bony S, Senior C, Stevens B, Taylor KE (2017) CMIP5 Scientific Gaps and Recommendations for CMIP6. Bull Am Meteor Soc 98(1):95–105. https://doi.org/10.1175/bams-d-15-00013.1

Sylla MB, Giorgi F, Pal JS, Gibba P, Kebe I, Nikiema M (2015) Projected changes in the annual cycle of high-intensity precipitation events over west Africa for the late twenty-first century*. J Clim 28(16):6475–6488. https://doi.org/10.1175/jcli-d-14-00854.1

Sylla MB, Elguindi N, Giorgi F, Wisser D (2016) Projected robust shift of climate zones over west Africa in response to anthropogenic climate change for the late 21st century. Clim Change 134(1–2):241–253. https://doi.org/10.1007/s10584-015-1522-z

Tamoffo AT, Dosio A, Vondou DA, Sonkoué D (2020) Process-based analysis of the added value of dynamical downscaling over central Africa. Geophys Res Lett. https://doi.org/10.1029/2020GL089702

Tamoffo AT, Amekudzi LK, Weber T, Vondou DA, Yamba EI, Jacob D (2021) Mechanisms of rainfall biases in two CORDEX-CORE regional climate models at rainfall peaks over central equatorial Africa. J Clim. https://doi.org/10.1175/JCLI-D-21-0487.1

Tapiador FJ, Navarro A, Levizzani V, García-Ortega E, Huffman GJ, Kidd C et al (2017) Global precipitation measurements for validating climate models. Atmos Res 197:1–20. https://doi.org/10.1016/j.atmosres.2017.06.021

Tapiador FJ, Roca R, Del Genio A, Dewitte B, Petersen W, Zhang F (2019) Is precipitation a good metric for model performance? Bull Am Meteor Soc 100(2):223–233. https://doi.org/10.1175/BAMS-D-17-0218.1

Taylor KE, Stouffer RJ, Meehl GA (2012) An overview of CMIP5 and the experiment design. Bull Amer Meteor Soc 93:485–498. https://doi.org/10.1175/BAMS-D-11-00094.1

Teichmann C, Jacob D, Remedio AR, Remke T, Buntemeyer L, Hoffmann P, Im E (2020) Assessing mean climate change signals in the global CORDEX-CORE ensemble. Clim Dyn. https://doi.org/10.1007/s00382-020-05494-x

Thorncroft CD, Hall NMJ, Kiladis GN (2008) Three-dimensional structure and dynamics of African easterly waves part III: genesis. J Atmos Sci 65:3596–3607. https://doi.org/10.1175/2008JAS2575.1

Tiedtke M (1989) A comprehensive mass flux scheme for cumulus parameterization in large-scale models. Mon Weather Rev 117(8):1779–1800. https://doi.org/10.1175/1520-0493(1989)117%3c1779:ACMFSF%3e2.0.CO;2

Titchner HA, Rayner NA (2014) The met office hadley centre sea ice and sea surface temperature data set, version 2: 1. Sea ice concentrations. J Geophys Res: Atmos 119(6):2864–2889. https://doi.org/10.1002/2013jd020316

Vizy EK (2002) Development and application of a mesoscale climate model for the tropics: influence of sea surface temperature anomalies on the west African monsoon. J Geophys Res. https://doi.org/10.1029/2001jd000686

Vizy EK, Cook KH (2001) Mechanisms by which gulf of Guinea and eastern north Atlantic sea surface temperature anomalies can influence African rainfall. J Clim 14(5):795–821. https://doi.org/10.1175/1520-0442(2001)0142.0.co;2

Vizy EK, Cook KH (2017) Seasonality of the Observed amplified Sahara warming trend and implications for Sahel rainfall. J Clim 30(9):3073–3094. https://doi.org/10.1175/jcli-d-16-0687.1

Vizy EK, Cook KH, Crétat J, Neupane N (2013) Projections of a wetter Sahel in the twenty-first century from global and regional models. J Clim 26(13):4664–4687. https://doi.org/10.1175/jcli-d-12-00533.1

Wang G, Eltahir EA (2000) Ecosystem dynamics and the Sahel drought. Geophys Res Lett 27(6):795–798. https://doi.org/10.1029/1999gl011089

Watterson I, Bathols J, Heady C (2014) What influences the skill of climate models over the continents? Bull Am Meteorol Soc 95(5):689–700. https://doi.org/10.1175/BAMS-D-12-00136.1

White J, Aiyyer A (2021) African easterly waves in an idealized general circulation model: instability and wave packet diagnostics. Weather Clim Dyn 2(2):311–329. https://doi.org/10.5194/wcd-2-311-2021

Wu M-LC, Reale O, Schubert SD, Suarez MJ, Thorncroft CD (2012) African easterly jet: barotropic instability, waves, and cyclogenesis. J Clim 25(5):1489–1510. https://doi.org/10.1175/2011jcli4241.1

Wu M, Nikulin G, Kjellström E, Belušić D, Jones C, Lindstedt D (2020) The impact of regional climate model formulation and resolution on simulated precipitation in Africa. Earth Syst Dyn 11(2):377–394. https://doi.org/10.5194/esd-11-377-2020

Xue Y, De Sales F, Lau WKM et al (2016) West African monsoon decadal variability and surface-related forcings: second west African monsoon modeling and evaluation project experiment (WAMME II). Clim Dyn 47:3517–3545. https://doi.org/10.1007/s00382-016-3224-2

Zhang L, Zhou T (2011) An assessment of monsoon precipitation changes during 1901–2001. Clim Dyn 37:279–296. https://doi.org/10.1007/s00382-011-0993-5

Zheng X, Eltahir EA (1998) The role of vegetation in the dynamics of west african monsoons. J Clim 11(8):2078–2096. https://doi.org/10.1175/1520-0442-11.8.2078